Journal of Hydrology: Regional Studies 21 (2019) 126–146

Contents lists available at ScienceDirect

Journal of Hydrology: Regional Studies

journal homepage: www.elsevier.com/locate/ejrh

Space-time disaggregation of precipitation and temperature across different climates and spatial scales

Korbinian Breinl[a,c,*], Giuliano Di Baldassarre[b,c]

[a] Institute of Hydraulic Engineering and Water Resources Management, Technische Universität Wien, Karlsplatz 13/222, 1040 Vienna, Austria
[b] Department of Earth Sciences, Uppsala University, Villavägen 16, 752 36 Uppsala, Sweden
[c] Centre of Natural Hazards and Disaster Science (CNDS), Uppsala, Sweden

ARTICLE INFO

Keywords:
Precipitation
Temperature
Disaggregation
Space-time scaling
Non-parametric
Method of fragments

ABSTRACT

Study region: This study focuses on two study areas: the Province of Trento (Italy; 6200 km^2), and entire Sweden (447000km^2). The Province of Trento is a complex mountainous area including subarctic, humid continental and Tundra climates. Sweden, instead, is mainly dominated by a subarctic climate in the North and an oceanic climate in the South.

Study focus: Hydrological predictions often require long weather time series of high temporal resolution. Daily observations typically exceed the length of sub-daily observations, and daily gauges are more widely available than sub-daily gauges. The issue can be overcome by disaggregating daily into sub-daily values. We present an open-source tool for the non-parametric space-time disaggregation of daily precipitation and temperature into hourly values called spatial method of fragments (S-MOF). A large number of comparative experiments was conducted for both S-MOF and MOF in the two study regions.

New hydrological insights for the region: Our experiments demonstrate the applicability of the univariate and spatial method of fragments in the two temperate/subarctic study regions where snow processes are important. S-MOF is able to produce consistent precipitation and temperature fields at sub-daily resolution with acceptable method related bias. For precipitation, although climatologically more complex, S-MOF generally leads to better results in the Province of Trento than in Sweden, mainly due to the smaller spatial extent of the former region.

1. Introduction

For hydrological predictions, the available records of precipitation and temperature are usually longest at daily resolution and daily gauges are more widely available than sub-daily gauges (Pui et al., 2012; Reynolds et al., 2017). Sub-daily records are often short, even in high-income countries (Di Baldassarre et al., 2006). In hydrology, characteristic space and time scales exist (Blöschl and Sivapalan, 1995; Skoien et al., 2003). In small catchments, for example, daily resolution often does not match the temporal scale of hydrological processes (Blöschl and Sivapalan, 1995; Reynolds et al., 2017). A high temporal resolution of precipitation is particularly desirable when modelling flash floods or local erosion (Lenderink and Van Meijgaard, 2008; Sikorska and Seibert, 2018). For example, the rapid response parameters of conceptual hydrological models largely depend on the temporal resolution of the precipitation input, and calibrating to sub-daily resolution can lead to better predictions (Wang et al., 2009). The spatial characteristics

* Corresponding author at: Institute of Hydraulic Engineering and Water Resources Management, Technische Universität Wien, Karlsplatz 13/222, 1040 Vienna, Austria.
E-mail address: breinl@hydro.tuwien.ac.at (K. Breinl).

https://doi.org/10.1016/j.ejrh.2018.12.002
Received 1 August 2018; Received in revised form 4 December 2018; Accepted 7 December 2018

of precipitation fields are likewise relevant (Arnaud et al., 2002; Evin et al., 2018; Zhang and Han, 2017), for example in trans-regional flood risk and water management (Leander et al., 2005), when modelling sewer systems in urban areas (Müller and Haberlandt, 2018) or for simulating the superposition of flood waves at the confluence of rivers (Hoch et al., 2017). A comprehensive literature review of the importance of spatial variability of precipitation in rainfall-runoff processes can be found in Tetzlaff and Uhlenbrook (2005). The temporal resolution of temperature is crucial for snow- and ice-dominated regions. Sub-daily temporal resolution is required for modelling melt-induced diurnal discharge variations (Hock, 2003; Simoni et al., 2011). Also, various process-oriented plant and soil models require sub-daily temperature forcing (Debele et al., 2007). Hourly resolution allows for evaluating processes such as leaf-level photosynthesis, canopy assimilation and transpiration (Boote et al., 2013). Simulating yields of the major annual food crops requires, at the minimum, hourly temperature (Porter and Semenov, 2005). Unlike in the case of precipitation, the role of consistent high-resolution temperature fields (i.e. the spatial signal) has received less attention in the literature. A possible explanation may be the high spatial correlation of temperature through its continuous, non-intermittent nature. While different authors have proposed sophisticated distributed energy balance models of high temporal resolution (e.g. Lehning et al., 2006; Rigon et al., 2006; Warscher et al., 2013), they are "less commonly used due to the need of spatially distributed hydrometeorological forcing data" (Mutzner et al., 2015).

To (i) overcome the aforementioned issue of less available sub-daily observations and (ii) still provide high-resolution forcing data for distributed process-oriented modelling, daily meteorological records can be disaggregated into finer time steps. The daily records for the disaggregation can be observed or synthetic, for instance from space-time stochastic weather models (e.g. Apipattanavis et al., 2007; Bardossy and Plate, 1992; Breinl et al., 2017a, 2015, 2013; Buishand and Brandsma, 2001; Clark et al., 2004; Evin et al., 2018). Such daily space-time weather generators can also be trained with climate model outputs to simulate future climates (Wilks, 1999).

Numerous models have been proposed for the univariate disaggregation from daily to finer sub-daily values at single sites, primarily for precipitation. Examples include Bartlett–Lewis/Neyman–Scott rectangular pulse algorithms (Khaliq and Cunnane, 1996; Rodriguez-Iturbe et al., 1987), random cascade algorithms (Carsteanu and Foufoula-Georgiou, 1996; Gupta and Waymire, 1993; Molnar and Burlando, 2005), the randomized Bartlett–Lewis model (Koutsoyiannis and Onof, 2001) or the more recent non-parametric method of fragments (MOF) (Mehrotra et al., 2012; Sharma and Srikanthan, 2006; Westra et al., 2012). Pui et al. (2012) provide a comprehensive overview of different univariate precipitation disaggregation techniques. Conversion from daily into sub-daily temperature is typically achieved by sinusoidal approaches when the daily maximum and minimum temperatures are available (Johnson and Fitzpatrick, 1977; Parton and Logan, 1981).

Independent univariate disaggregation of weather time series at each observation site leads to unrealistic weather fields lacking spatial consistence (Koutsoyiannis et al., 2003; Müller and Haberlandt, 2015). Koutsoyiannis et al. (2003) proposed a parametric space-time approach where several univariate (autoregressive) and multivariate precipitation models are implemented at different time scales. Müller and Haberlandt (2015) applied a modified microcanonical disaggregation model for precipitation based on Lisniak et al. (2013). First, Müller and Haberlandt (2015) disaggregated the precipitation independently at each site. Second, they used simulated annealing to transform the disaggregated and inconsistent precipitation fields into spatial consistency. Bardossy and Pegram (2016) proposed a space-time method for disaggregating daily precipitation to hourly intensities using a Gaussian copula-based model.

Increased attention has been recently dedicated to space-time approaches based on the idea of the univariate non-parametric method of fragments (MOF) (Mehrotra et al., 2012; Sharma and Srikanthan, 2006; Westra et al., 2012). The fundamental idea of MOF is disaggregate the day of interest using a similar candidate day (similarity can be derived in different ways, e.g. similar season, precipitation amount etc.) and impose the relative distribution (i.e. fragments) of the candidate day on the day of interest. Mezghani and Hingray (2009) applied a space-time version of MOF for disaggregating climate projections where potential candidates are selected from a temporal window, a method later on used in a similar way by Lu and Qin (2014). The best fragments are selected among these potential candidates using the Mahalanobis distance. The highest probability is assigned to the neighbor with the lowest deviation using the method presented in Lall and Sharma (1996). Li et al. (2018) presented a space-time approach based on MOF called "MUL", using daily regional precipitation means clustered into different intensity classes for identifying suitable candidates for the disaggregation. Although not developed for hourly disaggregation, Evin et al. (2018) presented a similar method for disaggregating spatial precipitation fields from a 3-day temporal resolution to a daily resolution. Candidate fragments are selected based on the season, class of intensity, and using a score of similarity computed across the precipitation fields.

In this paper, we propose a robust non-parametric method for the space-time disaggregation of precipitation and temperature. The method is another spatial interpretation of the non-parametric method of fragments (MOF) (hereafter called S-MOF). We applied S-MOF in two diverse study areas in terms of climates and spatial scales, which were the Province of Trento (Italy) (area 6200 km^2) and entire Sweden (area 447000km^2). Moreover, we examine the performance of a joint (i.e. multivariate) and separate disaggregation of precipitation and temperature, and demonstrate the impact of imbalances in available daily and sub-daily gauges using different interpolation techniques. In both study areas, S-MOF is able to reproduce spatially consistent precipitation and temperature fields with acceptable method related bias.

Non-parametric approaches have a long tradition in hydrology and have not only been applied in the temporal disaggregation of weather time series but also real-time flood forecasting (Brath et al., 2002), generation of stream flow time series (Lall and Sharma, 1996; Markovic et al., 2015) or stochastic weather generation (Brandsma and Buishand, 1998; Wojcik and Buishand, 2003). Such methods are usually characterized by a low level of complexity. Non-parametric approaches do not require data transformations or assumptions regarding the dependence structure of the data (Borgomeo et al., 2015). However, as they are fully data-driven, they can be sensitive to outliers (Villarini et al., 2008). Non-parametric methods also rely on a representative data sample. Despite their differences, non-parametric and parametric approaches share the same general problem: a too strong stratification compared to a

limited sample size may lead to a perfect fit with limited prediction power, whereas a weaker stratification (i.e. fewer parameters) implies a decrease of fitting performance but improved prediction skills.

The structure of the paper is as follows: Section 2 describes the proposed space-time disaggregation algorithm, Section 3 presents the design of real data experiments in the two study areas, Section 4 provides the related results and Section 5 provides a discussion and conclusions with recommendations for application.

2. Disaggregation algorithm

For the sake of clarity, we first introduce the basic concept of MOF at single sites for precipitation step by step, and then describe our spatial interpretation including the disaggregation of temperature (S-MOF).

2.1. Disaggregation of precipitation at single sites using MOF

The method of fragments (MOF) is a non-parametric disaggregation technique. The idea is to resample a vector of fragments that represents the relative distribution of sub-daily to daily precipitation (Pui et al., 2012). The number of fragments corresponds to the sub-daily temporal resolution used, i.e. if the disaggregation is conducted from daily to hourly values, the relative distribution of sub-daily values consists of 24 relative weights that sum up to 1. In the simulation, variability is introduced by a k-nearest neighbor algorithm. The procedure can be summarized as follows:

(i) Obtain the daily precipitation value R_t to disaggregate where t represents the date of the day. R_t may be the aggregated sum of the observed hourly time series (or taken from another source such as observed daily records or from a stochastic daily weather generator). Use the observational hourly records, $X_{i,m}$, to build daily time series R_i, where m is the hourly time step and i denotes the day (Eq. (1)).

$$R_i = \sum_{1}^{24} X_{i,m} \tag{1}$$

Form a time series with hourly to daily ratios (Eq. (2)).

$$f_{i,m} = \frac{X_{i,m}}{R_i} \tag{2}$$

(ii) Build a window with l days around the day t of the daily precipitation records. For example, if t represents the 1 st of January and $l = 14$, all days between the 18th of December and the 15th of January (from all available years) are considered for disaggregation. To avoid the recreation of the observations, the current year is discarded if the (aggregated) observed hourly records are used as the daily value R_t.

(iii) To account for the continuity of rainstorms (such as more persistent frontal rainstorms), only take into account days from step (ii) that correspond to the same class of wet/dry days of the neighboring days, according to the following four classes (Eq. (3)),

$$\begin{aligned}
&\text{Class(1) [dry,wet,dry]},\ R_j > 0 \,|\, (R_{j-1} = 0,\ R_{j+1} = 0) \\
&\text{Class(2) [wet,wet,dry]},\ R_j > 0 \,|\, (R_{j-1} > 0,\ R_{j+1} = 0) \\
&\text{Class(3) [dry,wet,wet]},\ R_j > 0 \,|\, (R_{j-1} = 0,\ R_{j+1} > 0) \\
&\text{Class(4) [wet,wet,wet]},\ R_j > 0 \,|\, (R_{j-1} > 0,\ R_{j+1} > 0)
\end{aligned} \tag{3}$$

where j denotes a day within the moving window around the specific date t for disaggregation.

(iv) Identify the class $c_t = (c_t \in (Class\ 1 - 4))$ to which R_t belongs.

(v) Identify the number of nearest neighbors $k = \sqrt{n}$ where n denotes the sample size of all days falling within the moving window and meeting the class criterion. Build a vector R_j from the absolute differences for all neighbors using $|R_j - R_t|$ for all $j = 1,2, \ldots, k$ and assign the highest probability p_j to the neighbor with the lowest deviation using (Eq. (4)) (Lall and Sharma, 1996).

$$p_j = \frac{1/j}{\sum_{i=1}^{k} 1/i} \tag{4}$$

Sample from Eq. (4) (inverse cumulative distribution function) using a uniformly distributed random number (0,1). Use the date of the sampled day and find the corresponding hourly ratios from $f_{i,m}$ and form the new disaggregated time series r_t for day t using Eq. (5).

$$r_t = R_t \times f_{i,m} \tag{5}$$

(vi) Repeat Step (ii) to Step (v) for each day t until the entire daily records are disaggregated.

An inherent property of MOF (and other block-bootstrap algorithms) is that the temporal correlation of the precipitation is

maintained within the disaggregated vectors of 24 h and discontinuities occur between blocks. Improvements to address this issue have been discussed (Sharma and Srikanthan, 2006), but are not further discussed here.

2.2. Transferring MOF into space for precipitation and temperature

The proposed non-parametric S-MOF model works as follows:

(i) Obtain the daily precipitation vector $R_{t,s}$ to disaggregate where t represents the date of the day and s individual sites of the observation network. As in the case of the univariate MOF, $R_{t,s}$ can come from the observed multi-site hourly records used for the disaggregation or from another source such as daily weather generators. Use the observational hourly records, $X_{i,m,s}$, to build daily time vectors $R_{i,s}$, where i denotes the day, m is the hourly time step and s is a site of the observation network (Eq. (6)).

$$R_{i,s} = \sum_{1,s}^{24} X_{i,m,s} \tag{6}$$

Form a time series of vectors with hourly to daily ratios (Eq. (7)).

$$f_{i,m,s} = \frac{X_{i,m,s}}{R_{i,s}} \tag{7}$$

(ii) Build a window with l days around the day t of the daily precipitation records. For example, if t represents the 1 st of January and $l = 14$, all days between the 18th of December and the 15th of January (from all available years) are considered for disaggregation. To avoid the recreation of the observations, the current year is discarded if the observations are used as the daily vector $R_{t,s}$.

(iii) Instead of using binary precipitation information, populate the matrix A_p with actual precipitation amounts (A'_p, Eq. (8)). The precipitation amounts are standardized beforehand with a square root standardization, which is preferable for positively skewed variables such as precipitation (Stephenson et al., 1999). The standardization led to an improved reproduction of dry and wet spells in our experiments. A standardization of the temperature did not lead to an improved performance and was thus not considered.

$$A'_p = \begin{bmatrix} R_{t-1,s_1} & R_{t-1,s_2} & \cdots & R_{t-1,s_n} \\ R_{t,s_1} & R_{t,s_2} & \cdots & R_{t,s_n} \\ R_{t+1,s_1} & R_{t+1,s_2} & \cdots & R_{t+1,s_n} \end{bmatrix}, \quad R_{t-1,s_n} \geq 0, \quad R_{t,s_n} > 0, R_{t+1,s_n} \geq 0 \tag{8}$$

Compare matrix A'_p to the values for disaggregation by building matrices B'_p for all days j within the moving window around the specific date (Eq. (9))t. Accordingly, also here the square root standardization must be applied.

$$B'_p = \begin{bmatrix} R_{j-1,s_1} & R_{j-1,s_2} & \cdots & R_{j-1,s_n} \\ R_{j,s_1} & R_{j,s_2} & \cdots & R_{j,s_n} \\ R_{j+1,s_1} & R_{j+1,s_2} & \cdots & R_{j+1,s_n} \end{bmatrix}, \quad R_{j-1,s_n} \geq 0, \quad R_{j,s_n} > 0, R_{j+1,s_n} \geq 0 \tag{9}$$

A separate (i.e. independent of the precipitation) disaggregation for the temperature is conducted accordingly, with the matrices A_t' and B_t' populated with the temperature observations (Eqs. (10) and (11)).

$$A'_t = \begin{bmatrix} T_{t-1,s_1} & T_{t-1,s_2} & \cdots & T_{t-1,s_n} \\ T_{t,s_1} & T_{t,s_2} & \cdots & T_{t,s_n} \\ T_{t+1,s_1} & T_{t+1,s_2} & \cdots & T_{t+1,s_n} \end{bmatrix}, \quad T_{t-1,s_n} \in \mathbb{R}\ , T_{t,s_n} \in \mathbb{R}, T_{t+1,s_n} \in \mathbb{R} \tag{10}$$

$$B'_t = \begin{bmatrix} T_{j-1,s_1} & T_{j-1,s_2} & \cdots & T_{j-1,s_n} \\ T_{j,s_1} & T_{j,s_2} & \cdots & T_{j,s_n} \\ T_{j+1,s_1} & T_{j+1,s_2} & \cdots & T_{j+1,s_n} \end{bmatrix}, \quad T_{j-1,s_n} \in \mathbb{R}, \ T_{j,s_n} \in \mathbb{R}, \ T_{j+1,s_n} \in \mathbb{R} \tag{11}$$

A joint disaggregation of precipitation and temperature was also tested, that is the matrices $A_p^{'}$ and $A_t^{'}$ as well as $B_p^{'}$ and $B_t^{'}$ were joined into the matrices $A_m^{'}$ and $B_m^{'}$ (Eqs. (12) and (13)) containing both meteorological variables.

$$A'_m = \begin{bmatrix} R_{t-1,s_1} & R_{t-1,s_2} & \cdots & R_{t-1,s_n} \\ R_{t,s_1} & R_{t,s_2} & \cdots & R_{t,s_n} \\ R_{t+1,s_1} & R_{t+1,s_2} & \cdots & R_{t+1,s_n} \\ T_{t-1,s_1} & T_{t-1,s_2} & \cdots & T_{t-1,s_n} \\ T_{t,s_1} & T_{t,s_2} & \cdots & T_{t,s_n} \\ T_{t+1,s_1} & T_{t+1,s_2} & \cdots & T_{t+1,s_n} \end{bmatrix},$$

$$R_{t-1,s_n} \geq 0, R_{t,s_n} > 0, R_{t+1,s_n} \geq 0, T_{t-1,s_n} \in \mathbb{R}, T_{t,s_n} \in \mathbb{R}, T_{t+1,s_n} \in \mathbb{R} \tag{12}$$

$$B'_m = \begin{bmatrix} R_{j-1,s_1} & R_{j-1,s_2} & \cdots & R_{j-1,s_n} \\ R_{j,s_1} & R_{j,s_2} & \cdots & R_{j,s_n} \\ R_{j+1,s_1} & R_{j+1,s_2} & \cdots & R_{j+1,s_n} \\ T_{j-1,s_1} & T_{j-1,s_2} & \cdots & T_{j-1,s_n} \\ T_{j,s_1} & T_{j,s_2} & \cdots & T_{j,s_n} \\ T_{j+1,s_1} & T_{j+1,s_2} & \cdots & T_{j+1,s_n} \end{bmatrix},$$

$$R_{j-1,s_n} \geq 0, R_{j,s_n} > 0, R_{j+1,s_n} \geq 0, T_{j-1,s_n} \in \mathbb{R}, T_{j,s_n} \in \mathbb{R}, T_{j+1,s_n} \in \mathbb{R} \quad (13)$$

If the entire day t is dry at all sites of the observation network, A'_m and B'_m reduce to T_{t,s_n} and T_{j,s_n}.The rationale behind the joint disaggregation was to examine whether using the precipitation and temperature from the same day for disaggregation would lead to a more consistent disaggregation of both variables, thereby maintaining the dry and wet temperatures.

(iv) Use a distance measure d to derive the similarities between A'_p ($A_t^{'}$) and all instances of $B_p^{'}$ ($B_t^{'}$), or in case of a joint disaggregation A'_w and B'_w. We used the Manhattan distance (Eq. (14)), which also turned out to work well with nearest neighbor algorithms for univariate precipitation disaggregation (e.g. Breinl et al., 2017b).

$$d(A', B') = \sum_{i=1}^{j} |A' - B'| \quad (14)$$

(v) Identify the number of nearest neighbors $k = \sqrt{m}$ where m denotes the number of days falling within the moving window. The distances are sorted for all $j = 1,2, \ldots, k$ and the highest probability p_j is assigned to the neighbor with the lowest deviation using Eq. (4).

(vi) Sample a neighbor using a uniformly distributed random number (0,1) from the inverse cumulative distribution function from Eq. (4). The date of the sampled day is used and the corresponding hourly ratios are applied at each site in the disaggregation. For the precipitation vectors, the new hourly time series $r_{i,s}$ are derived using Eq. (15).

$$r_{i,s} = R_{t,s} \times f_{i,m,s} \quad (15)$$

For the temperature, the disaggregation method is different. First, a time series of the absolute deviations between the hourly values and their mean is generated (Eq. (16))

$$g_{i,m,s} = Y_{i,m,s} - \bar{Y}_{i,m,s} \quad (16)$$

The new disaggregated temperature time series for day t is then derived with Eq. (17), using the daily mean temperature $T_{t,s}$:

$$t_{i,s} = T_{t,s} + g_{i,m,s} \quad (17)$$

This adapted method for the temperature (Eqs. (16) and (17)) ensures that the hourly distribution of negative and positive values in cold seasons is maintained after the disaggregation, and that the deviations between the input and disaggregated hourly values are kept constant over the 24 h, which is important for the temperature autocorrelation.

(vii) Repeat Step (ii) to Step (vi) for each day t until the entire daily records are disaggregated.

To reduce the impact of densely spaced sites of a network, in particular for precipitation, it can help to use Thiessen weights, which are then multiplied with the corresponding columns of the matrices A (Eqs. (8), (10) and (12)). However, Thiessen weights did not noticeably improve the results in the two study areas presented.

3. Data experiments and validation

3.1. Study area and data

We applied S-MOF to two different study areas. In the first study area, we used hourly precipitation and temperature records from 48 gauges in the North of Italy (Province of Trento, Fig. 1) covering a period of 15 years (1992–2006). The maximum distance between the sites is 104 km (area about 6200 km^2). The complex mountainous area in Italy comprises subarctic, humid continental and Tundra climates (Kottek et al., 2006). The total annual precipitation varies between 760 mm and 1500 mm (mean: 1100 mm) across all sites. The percentage of wet days varies between 31.6 and 47.2 (mean: 37.2). The mean annual temperature ranges from 0.6 °C to 8.5 °C (mean: 5.3 °C). The second study area is the entire country of Sweden (area of approximately 447000km^2, Fig. 1). For Sweden, 22 years (1996–2017) of simultaneous hourly precipitation and temperature time series were available (65 gauges). The maximum distance between sites is 1430 km. Accordingly, the density of the gauge station network in Italy is about 53 times higher. Sweden is mainly dominated by a subarctic climate in the North and an oceanic climate in the South (Kottek et al., 2006). The total annual precipitation varies between 398 mm and 1000 mm (mean: 577 mm). The percentage of wet days varies between 42.2 and 58.3 (mean: 50.6). The mean annual temperature ranges from -1.3 °C to 8.8 °C (mean: 4.6 °C). Both study areas are characterized by temperate and continental climates and snow processes are important.

3.2. Types of experiments and related methods

We conducted seven major types of experiments for S-MOF and three major experiments for MOF as a benchmark (Table 1). In

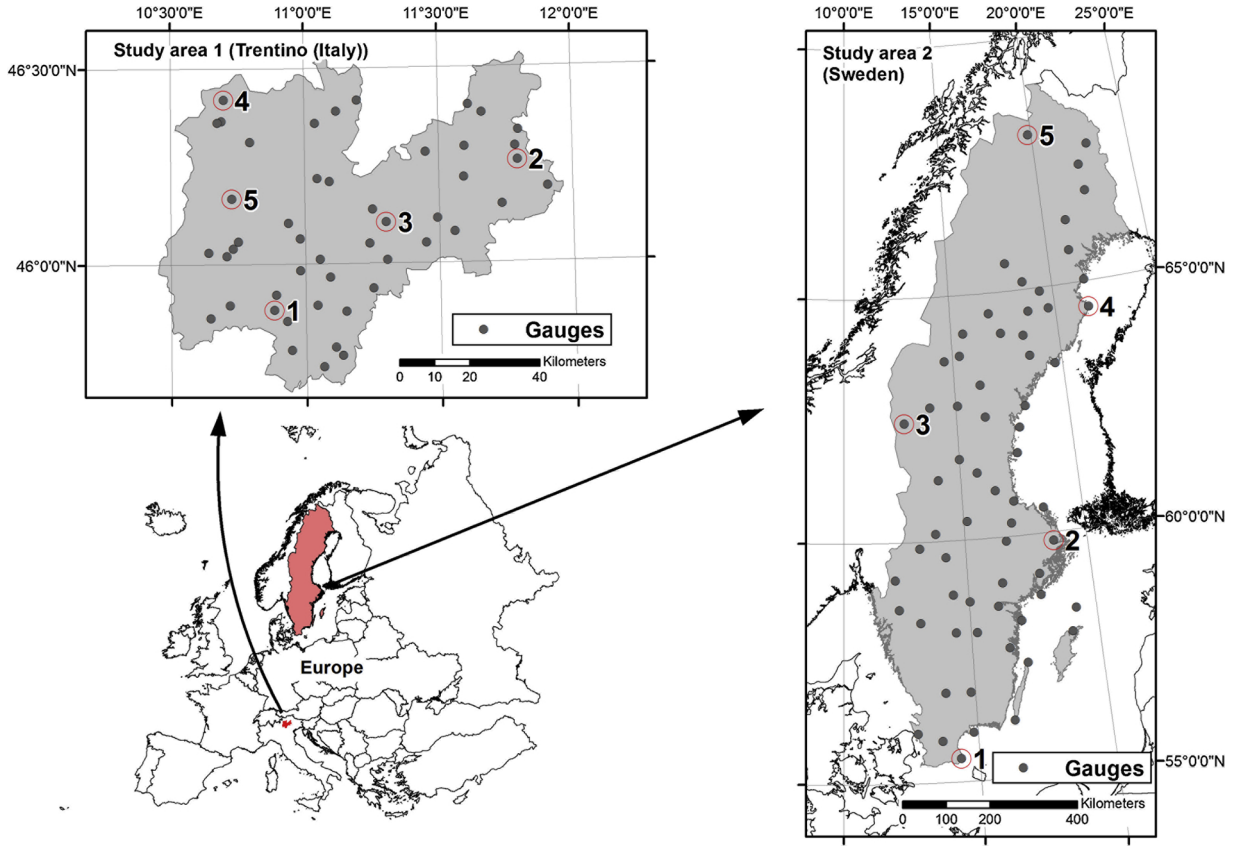

Fig. 1. Locations of the rain and temperature gauges in the Province of Trento (Italy) and Sweden. In Italy, 48 gauges provide simultaneous observations of hourly precipitation and temperature for the period 1992-2006. In Sweden, 65 gauges provide simultaneous observations for the period 1996-2017. The numbered gauges refer to sites used for plotting exemplary nonexceedance curves of precipitation (Section 4).

Table 1
Algorithms examined and related experiments for precipitation and temperature disaggregation including their abbreviations used in the article.

Algorithm / Experiment	Abbreviation in figures	S-MOF	MOF	MOF*
Full station network	S-MOF, MOF, MOF*	yes	yes	yes
10% missing data	M10	yes	–	–
30% missing data	M30	yes	–	–
Interpolation 70% of sites (advanced)	Int70	yes	–	–
Interpolation 50% of sites (advanced)	Int50	yes	yes	yes
Interpolation 30% of sites (advanced)	Int30	yes	–	–
Interpolation 50% of sites (simplistic)	Int50s	yes	yes	yes

addition, we applied S-MOF in a univariate setup (i.e. separate disaggregation at each site, hereinafter called MOF* (Table 1)). We limited the number of experiments for the univariate algorithms MOF and MOF* to keep the study concise. In all experiments, we conducted the disaggregation 50 times and compared observations with simulations.

To better understand the impact of missing data in the observation records, we randomly removed 10% and 30% of the entire observation days in each of the 50 simulations ("M10" and "M30", Table 1). Also, as described in the introduction, the number of available sub-daily gauges may be lower than the number of daily gauges. We thus tested the influence of a reduced gauge network by intentionally reducing the number of sub-daily sites for the disaggregation using S-MOF. To do so, we applied an advanced interpolation routine using 70%, 50% and 30% of the hourly gauges ("Int70", "Int50", "Int30", Table 1), and a simplified interpolation routine using 50% of the hourly gauges ("Int50s", Table 1). For MOF and MOF*, we only applied Int50 and Int50 s to keep the tests concise. To mimic the complexity of real-life data-availability, the network was randomly reduced to the required percentage in each of the 50 simulation runs.

In the advanced interpolation routine for precipitation, we first built 24-hour hyetographs for the site without hourly information (i.e. the removed site) from the three hyetographs h_n of three closest gauges with precipitation records. The three neighbouring hyetographs were weighted according to the inverse of their distance (w_n) to the site without hourly information (Eq. (18)).

$$h_{disagg} = w_1 \cdot h_1 + w_2 \cdot h_2 + w_3 \cdot h_3 \tag{18}$$

where h_1 is the 24-hour hyetograph of the first of the three nearest sites with precipitation records, w_1 is the inverse of the distance between the site of disaggregation and the first neighbouring site, and so forth. $w_1 + w_2 + w_3$ is scaled to 1.

As the hyetographs h_n may overlap in time (e.g. time lag from moving weather systems), there is the possibility of overestimating the number of wet hours at the site of disaggregation. For this reason, the final hyetograph was adapted by randomly cutting out a fraction of h_{disagg} with the weighted average length of each of the three neighbouring hyetographs. The weights for the lengths were again derived from the three distances. The starting hour of the fraction was randomly chosen within the total duration of h_{disagg}. This procedure turned out to avoid the simulation of too many wet hours at the site of disaggregation. The procedure was applied accordingly in the advanced temperature interpolation but without the step of cutting out a fraction (as temperature is continuous and non-intermittent). In the simplistic interpolation procedure (precipitation and temperature), we assigned each of the removed site to the closest site of the reduced network, i.e. our criterion of similarity was the spatial distance. There are other ways of selecting a suitable neighbouring site such as using the crossing distance, which penalizes the crossing of crests and valleys (Gottardi et al., 2012). Likewise, other general interpolation routines such as Kriging with external drift (KED) would be possible.

We focused on the following ten (non-spatial and spatial) statistical metrics to evaluate the algorithm performance at each site in regard to hourly precipitation:

- Extremes (50^{th}, 75^{th} and 99^{th} percentiles)
- Standard deviation (in mm)
- Skewness of the distribution of wet hours
- Mean length of dry spells
- Mean length of wet spells
- Lag1-autocorrelation
- Lag2-autocorrelation
- Inter-site correlation (spatial metric)
- Inter-site correlation lagged by one hour (spatial metric)
- Continuity ratio (spatial metric)

The continuity ratio c (Wilks, 1998) is a tool for assessing the quality of simulated precipitation and is defined as (Eq. (19)):

$$c = \frac{E(x_i | x_i > 0,\ x_j = 0)}{E(x_i | x_i > 0,\ x_j > 0)} \tag{19}$$

The continuity ratio defines the ratio of the mean of the precipitation at site i depending on whether site j is wet or dry. If the correlation between sites is high the continuity ratio will be relatively small, and if the correlation is low it will be relatively large.

For hourly temperature, we used the following six (non-spatial and spatial) statistical metrics for the evaluation at each site:

- Extremes (50^{th}, 75^{th} and 99^{th} percentiles)
- Standard deviation (in °C)
- Lag1-autocorrelation
- Lag2-autocorrelation
- Inter-site correlation (spatial metric)
- Inter-site correlation lagged by one hour (spatial metric)

In all experiments, the observed hourly values were first aggregated to daily values and then disaggregated using S-MOF, MOF and MOF*. We applied the three algorithms with a window of $l = 30$ (i.e. 60 days as without day t and 8 neighbors k (see 2.1 (ii) and (v)). All experiments described above were conducted twice for both study areas, one time with a separate disaggregation of precipitation and temperature (Eqs. (8)–(11)) and one time jointly, i.e. the same day was used for the disaggregation of precipitation and temperature (Eqs. (12) and (13)). As explained above, the motivation for the joint disaggregation was our hypothesis that the joint procedure would result in an improved simulation of hourly dry and wet temperatures. In the main paper, we present the main results for a separate disaggregation of precipitation and temperature. The reason is that the separate disaggregation scheme turned out – in contradiction to our hypothesis – to be preferable, which we further demonstrate in Section 4.3 where we compare results from the joint and separate disaggregation schemes. We present results based on the entire (annual) time series. Seasonal results can be obtained from the Supplementary Material.

4. Results

4.1. Precipitation

Fig. 2 shows the results for the separate disaggregation of precipitation in Italy. The boxplots for the observations are built from all sites of the observation network, the boxplots for the simulations are built from all sites and the mean of all 50 simulations. The dashed red line indicates the median of the observations, the boxes represent the 25th and 75th percentiles.

For the extremes, all algorithms and all experiments lead to a slight overestimation. S-MOF (full network) leads to a mean absolute error (MAE) of 0.44 (mean absolute percentage error (MAPE) 8.9), while MOF and MOF* lead to a MAE of 0.56 and 0.47 (MAPE 9.5 and 8.6). The slightly higher overestimation of the MAE with MOF is related to the reduced number of (potential) neighbors in the disaggregation, as the four binary classes (Eq. (3)) represent an additional constraint. This constraint does not exist in S-MOF and MOF*. An increasing number of missing values (10% and 30%) in S-MOF increases the bias in simulating extremes. The advanced interpolation outperforms the simplistic interpolation for all three algorithms. The results are similar for the standard deviation of hourly precipitation and the skewness of wet hours. While all algorithms and experiments lead to an overestimation of the observations, S-MOF tends to produce less bias. The improved performance of MOF* in comparison with MOF can again be explained by the additional constraint of binary classes in MOF.

For dry spells, the univariate MOF and MOF* algorithms lead to slightly better results in terms of the MAE (S-MOF 1.64, MOF 1.37, MOF* 1.00) and MAPE (S-MOF 4.6, MOF 3.9, MOF* 2.8). This observation does not apply to wet spells, where S-MOF performs better in terms of the MAE (S-MOF 0.16, MOF 0.31, MOF* 0.27) and MAPE (S-MOF 4.6, MOF 9.0, MOF* 7.8). The interpolation has a more pronounced effect with S-MOF compared to MOF and MOF*. While the advanced interpolation leads to better results of reproducing dry spells in S-MOF (Int50: MAE 1.20; Int50s: MAE 2.76), the simplistic interpolation leads to equally good results in the simulation of wet spells (Int50: MAE 0.21; Int50s: MAE 0.22). In general, the interpolation routines have a less pronounced impact on the simulation results with MOF and MOF* compared to S-MOF.

All algorithms tend to underestimate the autocorrelation of precipitation. However, S-MOF and MOF* perform better than MOF. For the lag1 autocorrelation, the MAE of S-MOF, MOF and MOF* is 0.04, 0.07 and 0.05 (MAPE: 6.8, 11.9 and 8.9). The reason is that MOF uses binary classes to simulate the continuity of rainstorms, while S-MOF and MOF* use the actual precipitation amounts. The advanced interpolation leads to better results when simulating the autocorrelation. Missing data increase the bias in S-MOF.

The key difference in the performance of S-MOF and the univariate algorithms becomes obvious when examining statistics related to the spatial characteristics of the precipitation fields, namely the inter-site correlations and the continuity ratio. Both univariate algorithms fail in reproducing the inter-site correlations by a pronounced underestimation, while the continuity ratio is clearly overestimated. For the inter-site correlation, S-MOF leads to a MAE of 0.02 (MOF 0.26, MOF* 0.25) and to a MAPE of 3.9 (MOF 57.2, MOF* 54.9). The differences are equally pronounced for the continuity ratio. The lack of skills of the univariate algorithms becomes even more obvious when using scatter plots for the spatial metrics from Fig. 2 (Fig. S1 in the Supplementary Material).

Fig. 3 shows the results for the separate disaggregation of precipitation for Sweden. For the extremes, unlike in Italy, the univariate algorithms MOF (MAE 0.14, MAPE 7.1) and MOF* (MAE 0.12, MAPE 6.6) perform better than S-MOF (MAE 0.32, MAPE 15.4). The same applies to the standard deviation of precipitation and the skewness. The reason is that in the significantly larger study area of Sweden the candidate vectors are characterized by a higher variability than in Italy. This is related to the higher heterogeneity of the climate. While missing values have a similar negative effect on the statistics as in Italy, interpolation routines generally lead to a more pronounced bias with S-MOF compared to MOF and MOF*, in particular for the standard deviation. The advanced interpolation routine produces less bias with all three algorithms.

Dry spells are comparatively well reproduced by all three algorithms. Wet spells are better reproduced with S-MOF compared to MOF and MOF*. While the interpolation has generally less impact on the simulation results with MOF and MOF*, it produces higher biases with S-MOF. Missing data do not significantly impact the simulation results with S-MOF. Dry spells are better reproduced with S-MOF when applying the simplistic interpolation routine. The opposite applies to wet spells, where the advanced interpolation routine leads to better results. With MOF and MOF*, the advanced interpolation routine reduces the bias for both dry and wet spells.

Unlike in Italy, S-MOF performs worse in simulating the autocorrelation of precipitation compared to MOF and MOF*. This can be explained by the increased heterogeneity of the climate and higher gauge distances, i.e. S-MOF does not find enough candidate vectors that are essentially similar to the vector of the day of disaggregation. In Italy, S-MOF performed better than the univariate algorithms. The advanced interpolation outperforms the simplistic interpolation with all three algorithms.

As in the case of Italy, the univariate algorithms have reduced skills in reproducing the spatial characteristics of the precipitation. In Sweden, the issue seems to be less pronounced, though. This can be explained by the significantly higher distances between sites, i.e. lower inter-site correlations. The deviations between the observations and the simulations are more pronounced for MOF and MOF*, better noticeable with scatter plots (Fig. S2 in the Supplementary Material). Fig. 4 shows the absolute error for the inter-site correlation between all possible pairs of sites and their distances. As can be seen with MOF, the error is higher for closer sites, i.e. the higher the correlation between station pairs the higher the error. S-MOF does not show this characteristic and produces an equally low bias across all station pair distances. The effect is much more pronounced in Italy than in Sweden due to the high inter-site correlations. In Sweden S-MOF also produces a slightly higher bias for closer sites.

To better understand the performance in the simulation of dry and wet spells, we also plotted their observed and simulated density. Fig. 5 shows the results for Italy and all three algorithms (full network up to a spell duration of 24 h). The patterns for all algorithms are similar. Longer wet spells tend to be underestimated, while longer dry spells tend to be overestimated. Important to notice is the similar performance of S-MOF compared to MOF and MOF*. Its ability to simulate consistent space-time precipitation fields does not noticeably impact the simulation of the length of dry and wet spells.

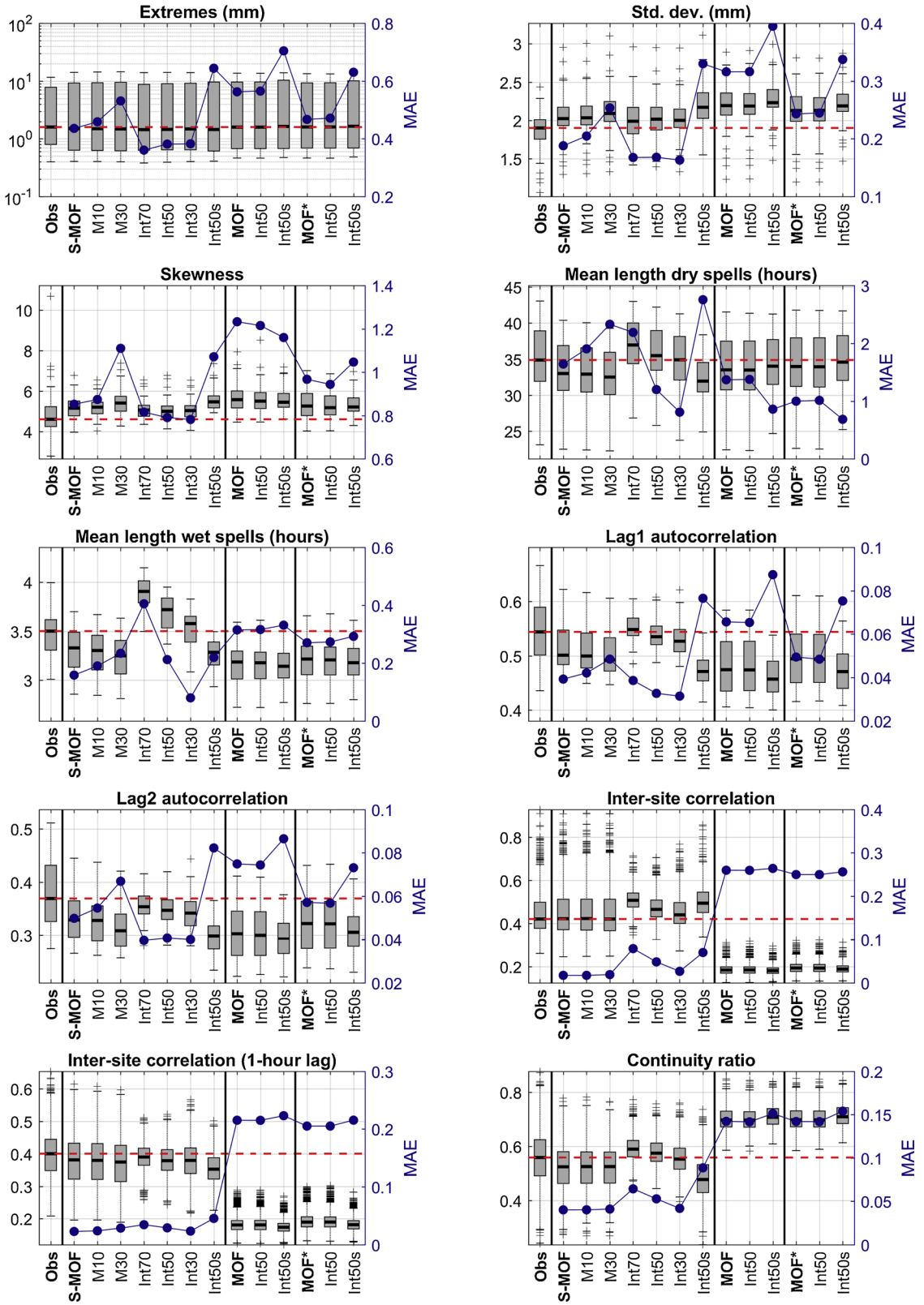

Fig. 2. Results from the precipitation disaggregation for ten metrics in Italy (separate disaggregation of precipitation and temperature). Boxplots for the observations (Obs) denote the statistics from all sites of the gauge network. Boxplots for the simulations are built from the mean of all 50 simulation runs and all sites, the dashed red line denotes the median of the observations. The simulation runs are split into results for S-MOF, MOF and MOF*. The abbreviations of the experiments are further explained in Table 1. The blue lines denote the mean absolute error (MAE) from all sites and simulations (For interpretation of the references to colour in this figure legend, the reader is referred to the web version of this article).

The results are slightly different for Sweden (Fig. 6). The most pronounced difference is the reduced skill of S-MOF to simulate longer wet spells. However, as in the case of Italy, all algorithms tend to underestimate longer wet spells. While shorter wet and dry spells are generally well reproduced by all algorithms, longer dry spells are overestimated except for S-MOF, which tends to slightly underestimate dry spells above a length of 20 h. Interestingly, the performance of S-MOF in regard to simulating the length of wet and dry spells appears to be of very good quality when comparing it to the skills of different (univariate) disaggregation schemes across Australia as presented in Pui et al. (2012) (Fig. 15 and Fig. 16 in Pui et al. (2012)), where most algorithms show higher biases, in particular for wet spells. In Pui et al. (2012), the univariate algorithm leading to the least bias is MOF.

Tables 2 and 3 give a summary of other important dry and wet spell characteristics in Italy and Sweden.

In Italy (Table 2), the performance of the three algorithms is comparable, with similar biases for the different metrics. The most remarkable difference is the higher bias of S-MOF regarding the skewness of dry and wet spells. The same applies to Sweden (Table 3), where the differences in reproducing the skewness of dry and wet spells are even more pronounced. A larger bias for the standard deviation of dry and wet spell durations can also be detected. The numbers for Sweden and S-MOF as provided in Table 3 are comparable with the results in Müller and Haberlandt (2015), who used a different model for simulating high-resolution space-time precipitation fields (see Section 1 of this article and Müller and Haberlandt (2015) for details), but at considerably smaller spatial scale (maximum site distance of about 200 km).

Seasonal results for the precipitation simulations can be obtained from the Supplementary Material (Figs. S3 and S4).

4.2. Temperature

The different algorithms and experiments have a less pronounced impact on the simulated temperature fields. Fig. 7 provides an overview of the performance of the three algorithms and all experiments for the separate disaggregation of temperature in Italy.

For the extremes, the standard deviation and the autocorrelations, the results of S-MOF, MOF and MOF* are comparable. Bias is being introduced by the interpolation routines, but the MAEs are low. As in the case of precipitation (Fig. 2), the bias of the interpolation routines is generally lower with the univariate algorithms MOF and MOF* compared to S-MOF, even though the differences are less pronounced compared to the precipitation simulations. While the advanced interpolation routine does not significantly improve the results with S-MOF, it performs better with MOF and MOF*. The autocorrelation of the temperature is comparatively well reproduced with all three algorithms: the bias introduced from missing data and interpolations is almost negligible considering the very low values of the MAE. As in the case of the precipitation, the inter-site correlations are underestimated with the two univariate algorithms, but to a much lower degree than for precipitation.

The results are very similar for Sweden (Fig. 8). Important to notice are the almost similar patterns (compared to Italy) of the MAE across the experiments and algorithms for the extremes, the standard deviation and the autocorrelation. The MAE is higher for the extremes and the standard deviation in Sweden with S-MOF, which can be explained by its larger spatial extent. Also important to notice is the higher bias when using the advanced interpolation. The simple interpolation routine appears to perform better for the autocorrelation and the inter-site correlations. While the inter-site correlations are generally better reproduced with S-MOF compared to MOF and MOF*, the differences are less pronounced in Sweden. As in the case of precipitation, this can be explained with the lower inter-site correlations due to the higher spatial distances between sites.

In general, the MAEs for the temperature are small across all algorithms and experiments.

Table 4 provides an overview of all results (MAPE) for S-MOF, MOF and MOF* (full network simulated), both meteorological variables and study areas, split into non-spatial and spatial metrics.

4.3. Separate and joint disaggregation in comparison

As explained in the Section 3.2, we conducted all experiments twice. One time with a separate disaggregation of precipitation and temperature (Eqs. (8)–(11)) and another time jointly, i.e. the same day from the observations was used for the disaggregation of precipitation and temperature (Eqs. (12) and (13)). Our hypothesis was that a joint disaggregation may lead to a better reproduction of the dry and wet temperatures with S-MOF.

Fig. 9 shows the results (MAE) split into dry and wet temperatures for both study areas. What first becomes obvious is that the joint disaggregation of precipitation and temperature is not able to significantly improve the dry and wet temperatures. The MAEs are comparable for both approaches in both study areas. In general, the MAE is lower for the dry temperature compared to the wet temperature due to the higher number of dry hours in the observations. When simulating the full observation networks in Italy, a joint disaggregation leads to marginally better results for the dry and wet temperature. Interpolation routines introduce additional bias. The highest bias of simulating dry temperatures is caused by missing values. In Sweden, in contradiction to our aforementioned hypothesis, a separate disaggregation even leads to a better reproduction of the dry and wet temperature across algorithms and experiments.

Most importantly, the joint disaggregation has a significant impact on the performance of the precipitation and temperature specific statistics already shown in Figs. 2, 3, 7 and 8. A noticeable decrease in the performance when conducting a joint disaggregation in Italy can be depicted from Fig. 10 (precipitation) and Fig. S5 in the Supplementary Material (temperature), which show the MAE from both disaggregation strategies in Italy. For the precipitation (Fig. 10), almost all metrics suffer from a joint disaggregation.

For the temperature in Italy, a joint disaggregation likewise decreases the performance. A marginal improvement can be detected for the univariate algorithms MOF and MOF* and the inter-site correlations.

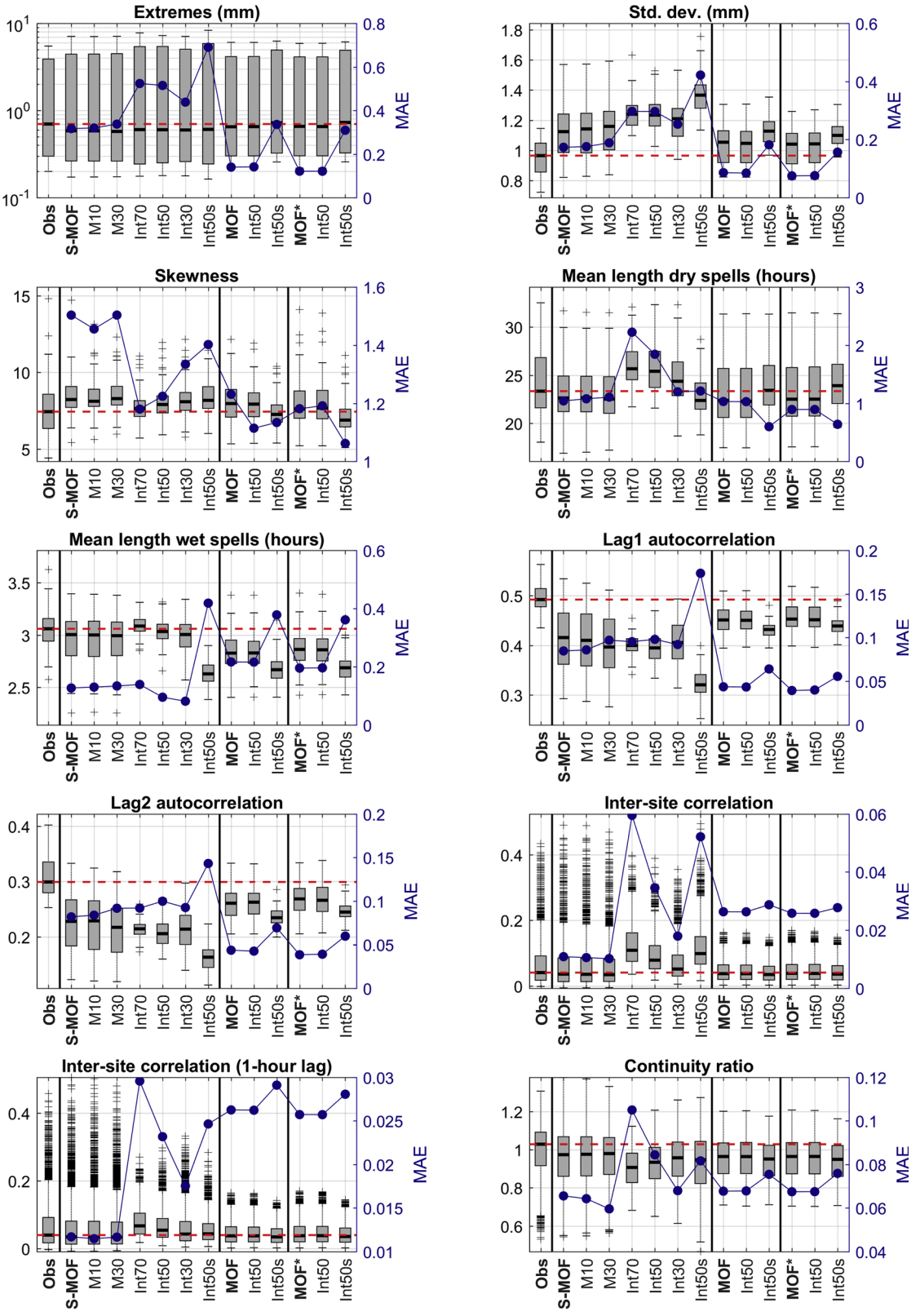

(caption on next page)

Fig. 3. Results from the precipitation disaggregation for ten metrics in Sweden (separate disaggregation of precipitation and temperature). Boxplots for the observations (Obs) denote the statistics from all sites of the gauge network. Boxplots for the simulations are built from all 50 simulation runs and all sites, the dashed red line denotes the median of the observations. The simulation runs are split into results for S-MOF, MOF and MOF*. The abbreviations of the experiments are further explained in Table 1. The blue lines denote the mean absolute error (MAE) from all sites and simulations (For interpretation of the references to colour in this figure legend, the reader is referred to the web version of this article).

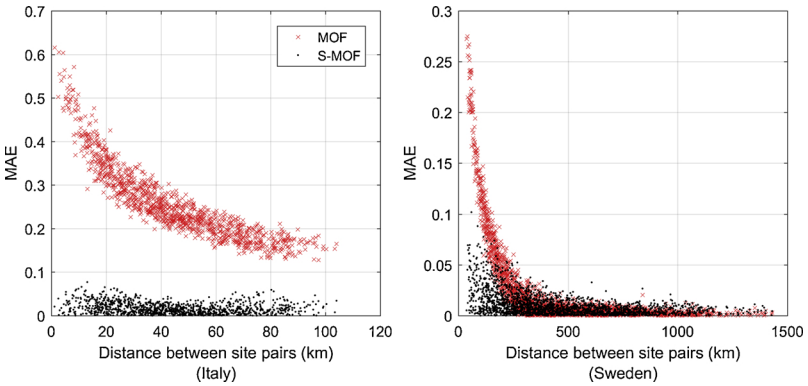

Fig. 4. Mean absolute error (MAE) from simulating the inter-site correlations plotted for S-MOF and MOF and all possible station pairs and their distances (Italy and Sweden).

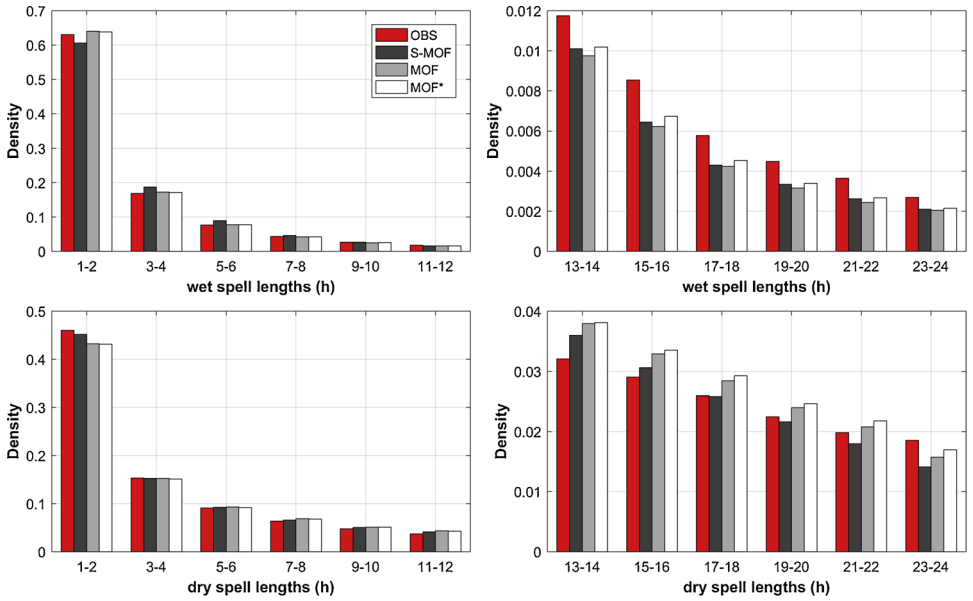

Fig. 5. Observed and simulated densities of wet and dry spells in 1st and 2nd rows (increasing spell length from left to right) with S-MOF, MOF and MOF* in Italy. Bars denote the mean of all sites and the 50 simulation runs.

For Sweden, the differences are less pronounced for S-MOF and precipitation (Fig. S6 in the Supplementary Material). The univariate algorithms MOF and MOF* however lead to significantly higher biases for extremes, the standard deviation and the autocorrelation of precipitation in a joint disaggregation. The differences for the temperature are less pronounced except for the simple interpolation routine with MOF and MOF*, where the bias is significantly higher compared to the advanced interpolation routine (Fig. S7 in the Supplementary Material).

The negative impact of the joint disaggregation also becomes noticeable when examining nonexceedance curves of hourly precipitation. Figs. 11 and 12 show the non-exceedance curves of hourly precipitation for the separate (Fig. 11) and joint (Fig. 12) disaggregation of precipitation for five selected sites across the Italian study area (see Fig. 1 for the selected five sites).

As can be depicted from Fig. 11, all three algorithms reproduce the nonexceedance probabilities well. A slight overestimation of extremes can be identified for all algorithms. All three algorithms produce values below the gauge station measuring accuracy, a well-known characteristic of disaggregation models. The joint disaggregation of precipitation and temperature introduces a higher bias in the nonexceedance curves (Fig. 12). While the increased bias for S-MOF is not particularly pronounced but still recognizable (e.g. Site

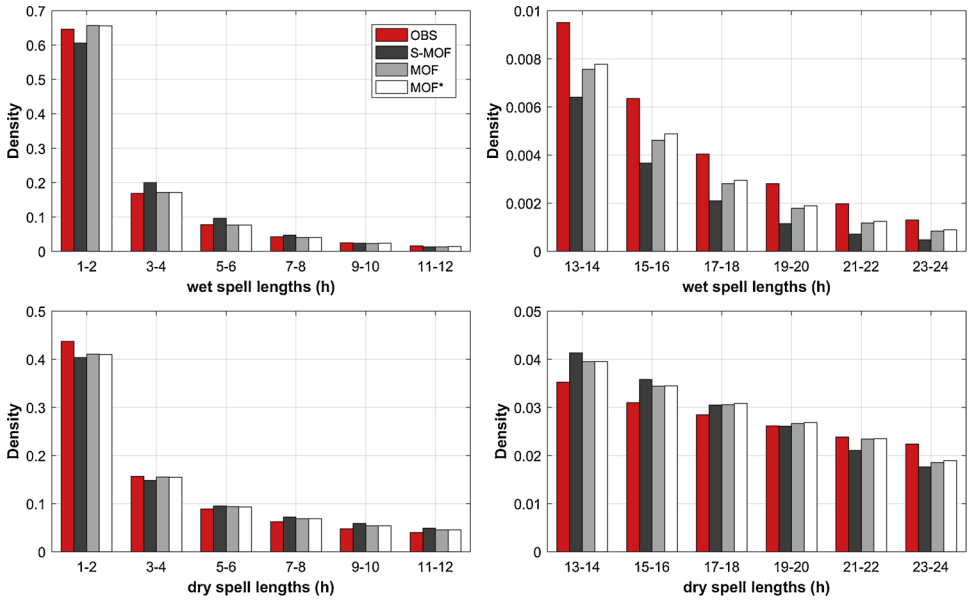

Fig. 6. Observed and simulated densities of wet and dry spells in 1st and 2nd rows (increasing spell length from left to right) with S-MOF, MOF and MOF* in Sweden. Bars denote the mean of all sites and the 50 simulation runs.

Table 2
Relative error and MAE for different wet and dry spell characteristics with S-MOF, MOF and MOF* (Italy).

	Relative error (%)			MAE		
Spell characteristics	S-MOF	MOF	MOF*	S-MOF	MOF	MOF*
Wet spell duration	−4.6	−9.0	−7.8	0.2	0.3	0.3
Std. dev.	−15.8	−16.3	−14.3	0.7	0.7	0.7
Skewness	−7.6	−2.2	−3.2	0.3	0.2	0.2
Wet spell amount	−4.6	−4.4	−3.3	0.2	0.2	0.2
Std. dev.	−11.5	−9.9	−8.3	1.2	1.0	0.9
Skewness	−7.0	−6.0	−5.7	0.5	0.4	0.4
Dry spell duration	−4.6	−3.9	−2.8	1.6	1.4	1.0
Std. dev.	−0.5	−1.9	−1.7	1.4	1.6	1.4
Skewness	4.8	2.3	2.2	0.3	0.2	0.1
Fraction of dry intervals	1.9	1.8	1.8	0.0	0.0	0.0

Table 3
Relative error and MAE for different wet and dry spell characteristics with S-MOF, MOF and MOF* (Sweden).

	Relative error (%)			MAE		
Spell characteristics	S-MOF	MOF	MOF*	S-MOF	MOF	MOF*
Wet spell duration	−3.5	−7.1	−6.4	0.1	0.2	0.2
Std. dev.	−22.4	−15.0	−13.7	0.8	0.5	0.5
Skewness	−30.8	−13.3	−13.1	1.1	0.5	0.5
Wet spell amount	−3.5	−4.6	−4.0	0.1	0.1	0.1
Std. dev.	−13.3	−8.1	−7.1	0.5	0.3	0.3
Skewness	−10.0	−5.6	−5.0	0.7	0.5	0.5
Dry spell duration	−3.5	−4.3	−3.7	1.1	1.0	0.9
Std. dev.	2.9	−2.4	−2.2	2.4	1.1	1.0
Skewness	8.1	2.7	2.5	0.4	0.1	0.1
Fraction of dry intervals	2.6	1.9	1.9	0.0	0.0	0.0

4 and Site 5 upper 5%), the deviations are generally more pronounced for the univariate algorithms MOF and MOF*. The results are similar for the Sweden (Figs. S8 and S9 in the Supplementary Material).

The general tendency of a decrease in performance across the algorithms and study areas when applying the joint disaggregation scheme appears to be reasonable: the joint algorithm considers both the distances to the precipitation and temperature candidates (Eqs. (12) and (13)), i.e. the algorithm considers the smallest common denominator for both precipitation and temperature. However, we also examined the inter-variable correlation between precipitation and temperature, which on average is 0.11 in Italy and 0.21 in

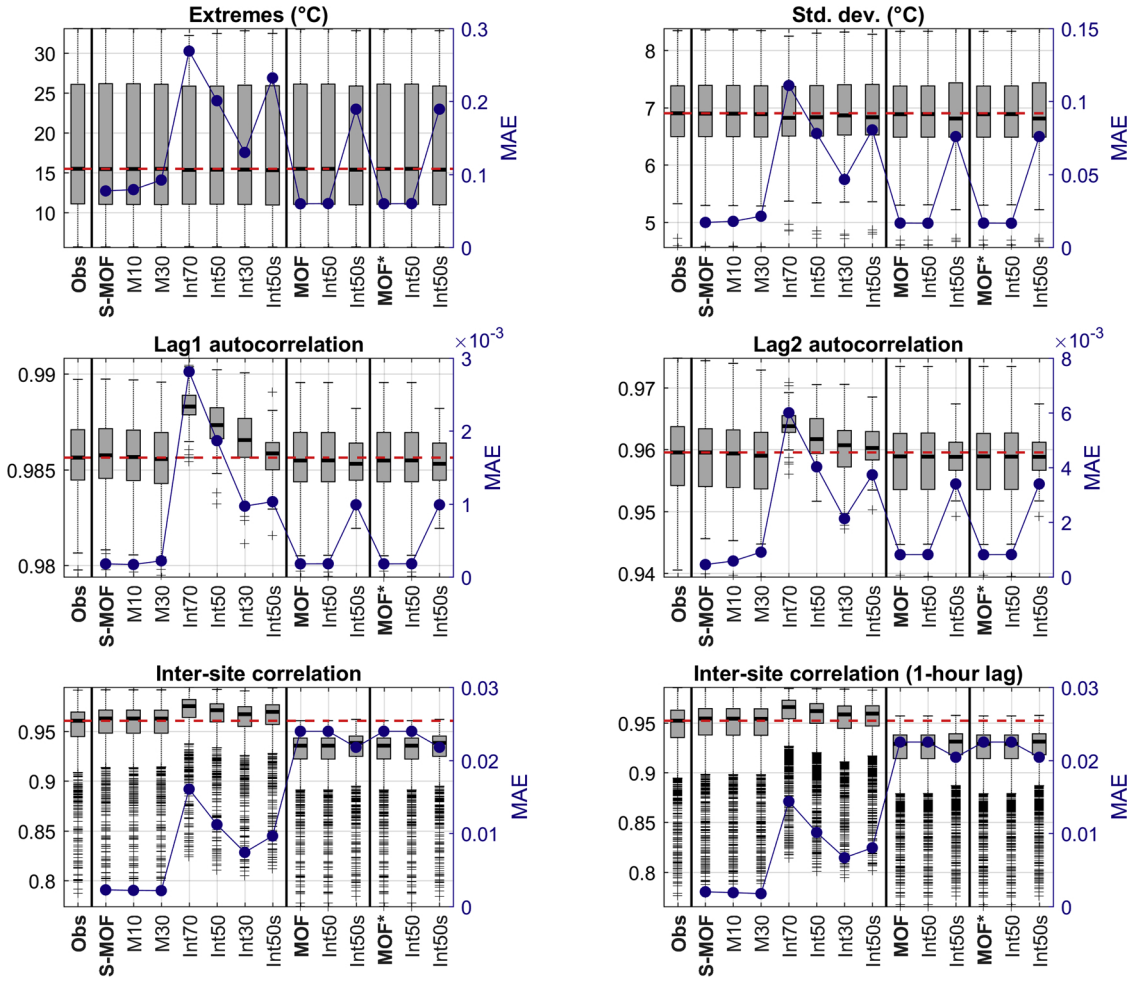

Fig. 7. Results from disaggregation for six metrics for temperature in Italy (separate disaggregation of precipitation and temperature). Boxplots for the observations (Obs) denote the statistics from all sites of the gauge network. Boxplots for the simulations are built from the mean of all 50 simulation runs and all sites, the dashed red line denotes the median of the observations. The simulation runs are split into results for S-MOF, MOF and MOF*. The abbreviations of the experiments are further explained in Table 1. The blue lines denote the mean absolute error (MAE) from all sites and simulations (For interpretation of the references to colour in this figure legend, the reader is referred to the web version of this article).

Sweden (Pearson correlation). When using the separate disaggregation in Italy, the inter-variable correlation was underestimated by 42.6% (S-MOF full station network), which reduced to a 24.9% underestimation with the joint approach. In Sweden, differences were less pronounced (underestimation in separate simulation 25.4%, in joint simulation 24.1%). However, given the overall decrease in performance and the fact that the dry and wet temperatures are not significantly better reproduced, a joint disaggregation of precipitation and temperature is not recommended and our original hypothesis of improved simulations of dry and wet temperatures using the same day has to be rejected.

5. Discussion and conclusions

For precipitation, S-MOF generally leads to better results at smaller spatial scale (Italy) compared to very large spatial scales (Sweden). At small spatial scale, S-MOF even outperforms the univariate MOF and MOF* algorithms with the exception of simulating dry spells and a higher bias of the skewness of the dry and wet spell durations. S-MOF performs generally well at small scale as the candidate vectors in the resampling algorithm tend to be similar (homogenous climate at small scale). With larger spatial scales, the climate and precipitation becomes more heterogeneous in space and time, i.e. the daily (and hourly) snapshots of precipitation have a higher spatial variability, leading to higher model biases. The univariate algorithms fail at reproducing the spatial characteristics of the precipitation. This shortcoming is more pronounced when facing high inter-site correlations, such as in smaller (and more densely gauged) study areas. As reproducing the spatial characteristics of the precipitation with S-MOF at very large spatial scales comes along with reduced skills in simulating other precipitation characteristics (e.g. standard deviation and autocorrelation), univariate models across such large domains appear to be a good alternative. Interpolation with the proposed advanced interpolation routine

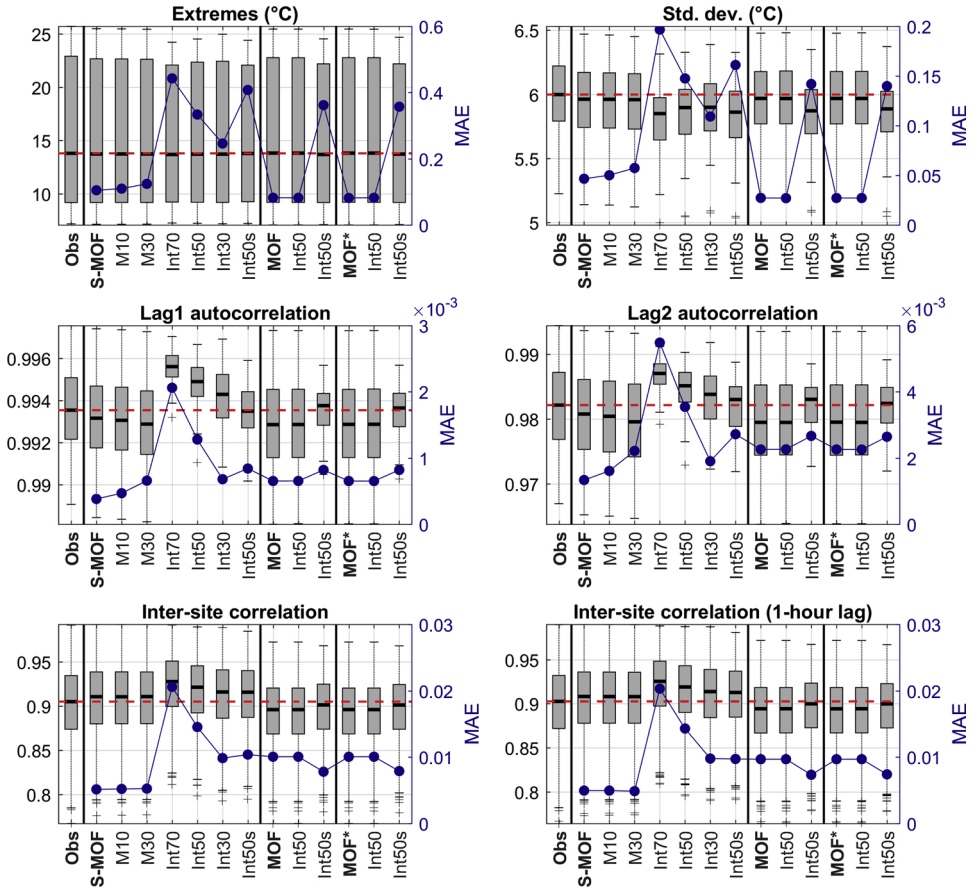

Fig. 8. Results from disaggregation for six metrics for temperature in Sweden (separate disaggregation of precipitation and temperature). Boxplots for the observations (Obs) denote the statistics from all sites of the gauge network. Boxplots for the simulations are built from the mean of all 50 simulation runs and all sites, the dashed red line denotes the median of the observations. The simulation runs are split into results for S-MOF, MOF and MOF*. The abbreviations of the experiments are further explained in Table 1. The blue lines denote the mean absolute error (MAE) from all sites and simulations (For interpretation of the references to colour in this figure legend, the reader is referred to the web version of this article).

Table 4
Mean absolute percentage error (MAPE) averaged over all non-spatial and spatial (see section 3.2.) metrics for both study areas, precipitation and temperature, separate and joint disaggregation schemes, and for the three algorithms S-MOF, MOF and MOF* (full network simulated).

Variable	Disaggregation scheme	Algorithm	Italy		Sweden	
			Non-spatial metrics	Spatial metrics	Non-spatial metrics	Spatial metrics
precipitation	separate	S-MOF	9.4	5.5	15.3	21.6
		MOF	14.0	46.6	9.5	25.5
		MOF*	11.0	45.0	8.6	25.4
	joint	S-MOF	18.1	8.7	16.4	21.4
		MOF	26.1	53.6	23.3	30.0
		MOF*	22.2	51.3	19.4	28.4
temperature	separate	S-MOF	0.2	0.2	0.4	0.6
		MOF	0.2	2.4	0.3	1.1
		MOF*	0.2	2.4	0.3	1.1
	joint	S-MOF	1.3	0.4	0.5	0.5
		MOF	0.5	2.2	0.3	1.0
		MOF*	0.5	2.2	0.3	1.0

leads to better results for most metrics. In future research it may be worth investigating the impact of more sophisticated interpolation routines such as KED. For temperature, simulations with S-MOF are generally more robust producing less bias than for precipitation, which can be explained by the continuous, non-intermittent nature of temperature. Interpolation routines applied to the temperature have less impact on the simulation results and the simplistic interpolation routine leads to good results.

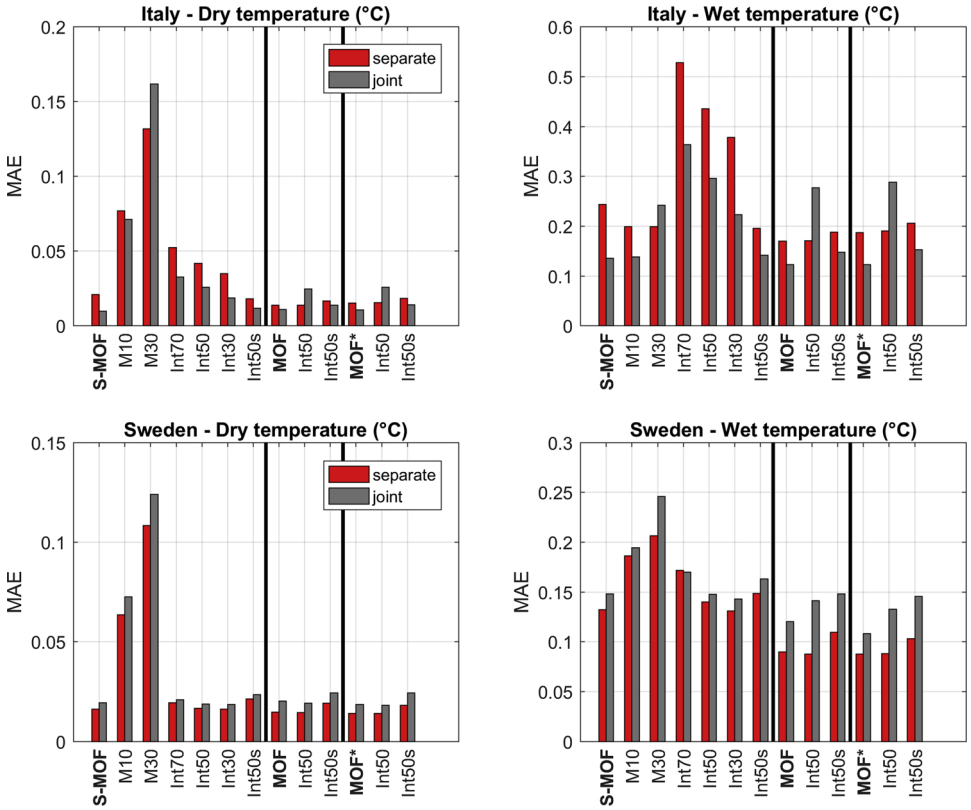

Fig. 9. Comparison of the mean absolute error (MAE) for the simulated dry and wet temperatures in Italy and Sweden from a separate and joint precipitation and temperature disaggregation. The simulation runs are split into results for S-MOF, MOF and MOF*. The abbreviations of the experiments are further explained in Table 1.

From a practical point of view, different biases produced by S-MOF have different implications for applications in impact studies. At small scale, the slight overestimation of precipitation extremes appears to be negligible, also for simulating extreme events such as flash floods. At larger scale, the overestimation of extremes increases. Here, while the simulation of large scale river floods and water balance simulations may be less affected, the simulation of flash floods in small catchments may become more problematic. S-MOF may thus be applied at smaller scale when such small scale extreme events are in focus. In that context, sensitivity studies only using a subset of sites for the disaggregation (not shown here) revealed a less pronounced bias in simulating extremes. The bias in simulating dry and wet spells appears to be acceptable with all algorithms (also when applying interpolation). However, it should be tested what the implications are by applying S-MOF and univariate alternatives in coupled rainfall-runoff frameworks. A high bias in the space-time simulation of the water-balance and spatial extreme events can be expected at small scale when using univariate precipitation models instead of S-MOF. This has for example been demonstrated by Müller and Haberlandt (2018), who compared univariate and multivariate disaggregation approaches and observed unrealistic flood volumes when ignoring spatial consistency. Regardless of the different metrics and their implications, one must also be aware that the simulated time series will eventually be interpolated for distributed impact modeling, which is another source of uncertainty that may increase or decrease the bias from the disaggregation algorithms. The bias from the temperature simulations seems to be less problematic. However, missing data and interpolation routines introduce higher biases. Also here, it is difficult to speculate and sensitivity studies using an exemplary catchment will help, for example by using sub-daily precipitation and temperature generated at large (with higher bias) and small scale (lower bias) to understand the impact of both input datasets. It would be interesting for further research to test S-MOF with different sub-daily temporal resolutions (e.g. 3 or 6 h).

An important finding of the study is that precipitation and temperature should be disaggregated separately. A joint disaggregation of both variables does not lead to a (significantly) better reproduction of dry and wet temperatures and introduces a significantly higher bias in both the precipitation and temperature simulations. Furthermore, MOF* appears to be an interesting alternative to MOF and leads to a reduced bias compared to MOF for various statistics.

The proposed method has some limitations: (i) the parameters of S-MOF are derived from observations and it is assumed that these parameters remain valid in the future as for the vast majority of disaggregation algorithms (Pui et al., 2012). The assumption of stationarity has been widely discussed in the literature (e.g. Luke et al., 2017; Milly et al., 2008; Montanari and Koutsoyiannis, 2014; Serinaldi and Kilsby, 2015). Montanari and Koutsoyiannis (2014) argue that any system is characterized by variability that cannot be explained and that physically based stochastic models assuming stationarity remain robust and useful tools for hydrological risk

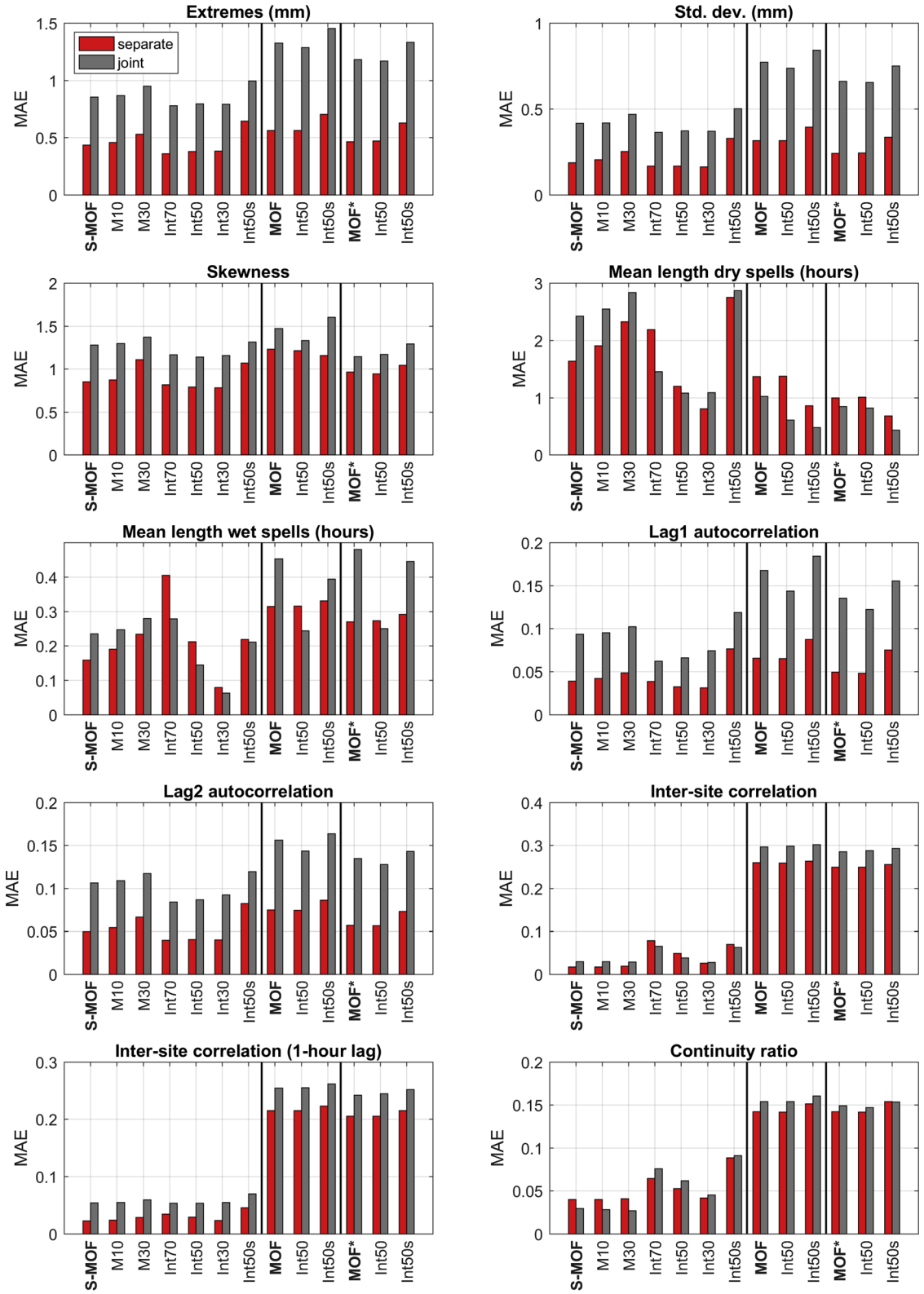

Fig. 10. Comparison of the mean absolute error (MAE) from disaggregation for ten metrics for precipitation in Italy (separate and joint disaggregation of precipitation and temperature). The bar plots show the MAE between the observations (all sites) and the mean of the 50 simulations conducted (all sites). The simulation runs are split into results for S-MOF, MOF and MOF*. The abbreviations of the experiments are further explained in Table 1.

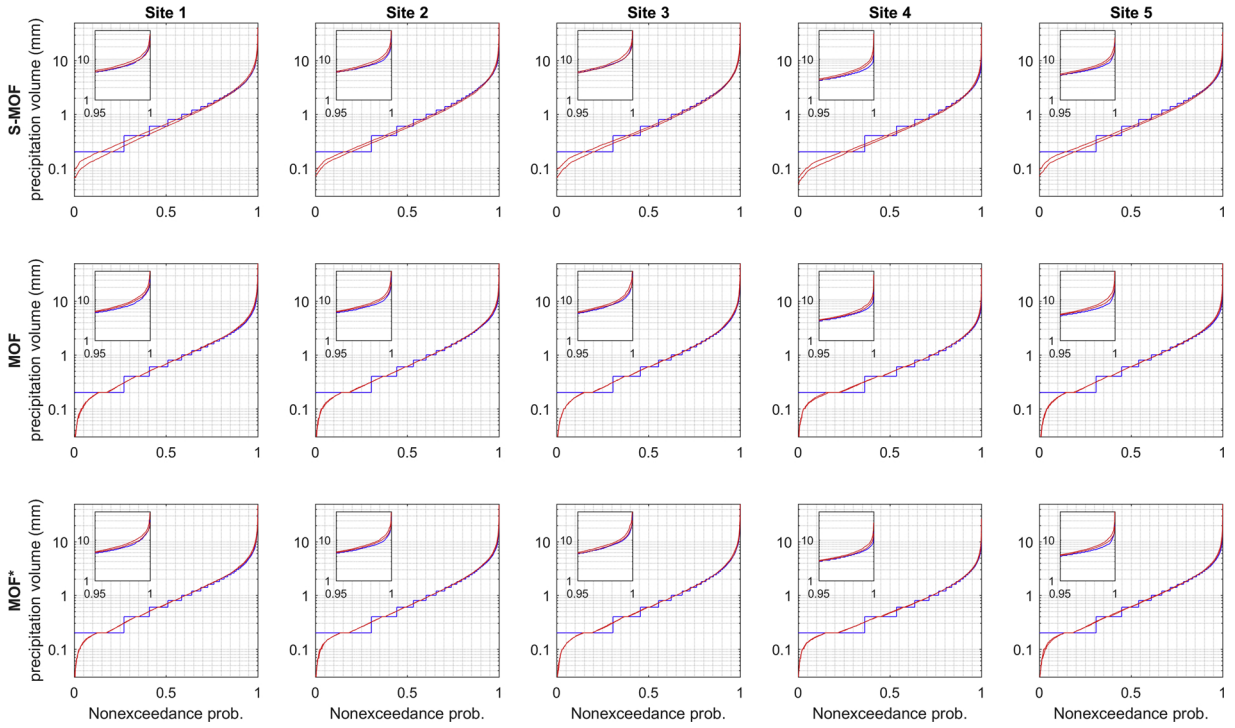

Fig. 11. Nonexceedance curves of the observed and disaggregated time series for S-MOF, MOF and MOF* (separate disaggregation of precipitation and temperature) and five selected sites across the Italian study area. Blue lines represent the observations (wet hours), red lines represent the envelope curves of the 50 simulations. The detailed plots represent the upper 5%. The sites of the plots refer to the highlighted gauges in Fig. 1 (For interpretation of the references to colour in this figure legend, the reader is referred to the web version of this article).

assessment. Serinaldi and Kilsby (2015) state that scientists should be careful when using nonstationary approaches due to the increased complexity and uncertainty and that non-stationary approaches are not suitable for the often short observation time series. Luke et al. (2017) show that stationary methods are more robust than non-stationary ones unless there is clear information about major physical changes in the river basin. As the length of available sub-daily observation time series is short in many places around the world, the assumption of stationarity appears to be reasonable, but should be tested whenever possible. In that context, further research could look into ways of modifying and applying S-MOF for future climate projections. One of the key challenges behind such an attempt is that the projected increase of hourly precipitation extremes may exceed the expectations from changes in the temperature (Clausius-Clapeyron relation) (Lenderink and Van Meijgaard, 2008). This behavior should be taken into account. As the future climate will be warmer, fragments equating to extreme daily precipitation will be different than in the current climate, which is for example related to changing storm dynamics in warming temperatures (Wasko and Sharma, 2015). Using an averaged temperature anomaly as an additional covariate in selecting the day for resampling may be an avenue to make the model more robust for disaggregating climate projections; (ii) as addressed in Section 2.1 S-MOF, MOF and other (block)bootstrap methods have the inherent limitation of discontinuities between blocks as a general feature. While considering the day before and after in finding neighbours reduces the risk of generating pronounced artefacts, another strategy to cope with the issue could be implementing additional constraints for selecting a suitable day for disaggregation to ensure smoother transitions between blocks. Such efforts would however increase the number of parameters while facing comparatively short time series, thus potentially reducing the prediction power of the model; (iii) the application of S-MOF is limited to regions where continuous sub-daily observations are available. In the case of our experiments, simultaneous records at all sites were available. The algorithm could be modified so that single missing records in the hourly observations vectors are complemented using an interpolation routine. However, this step can also be considered to be part of the data preparation before applying S-MOF; (iv) we tested S-MOF in different precipitation rich climates across different spatial scales. Disaggregating precipitation with S-MOF in arid climates may lead to issues, as the candidate vectors may become highly diverse, i.e. the algorithm may not find a sufficient number of candidates for the disaggregation. However, in arid climates, correlations between sites may generally be low so that spatial methods are not needed.

In summary, the proposed open-source S-MOF disaggregation algorithm is a straightforward and robust method for generating sub-daily precipitation and temperature fields that are consistent in space and time. S-MOF complements the available spatial disaggregation techniques currently available and has potential for various applications in engineering and water resources research.

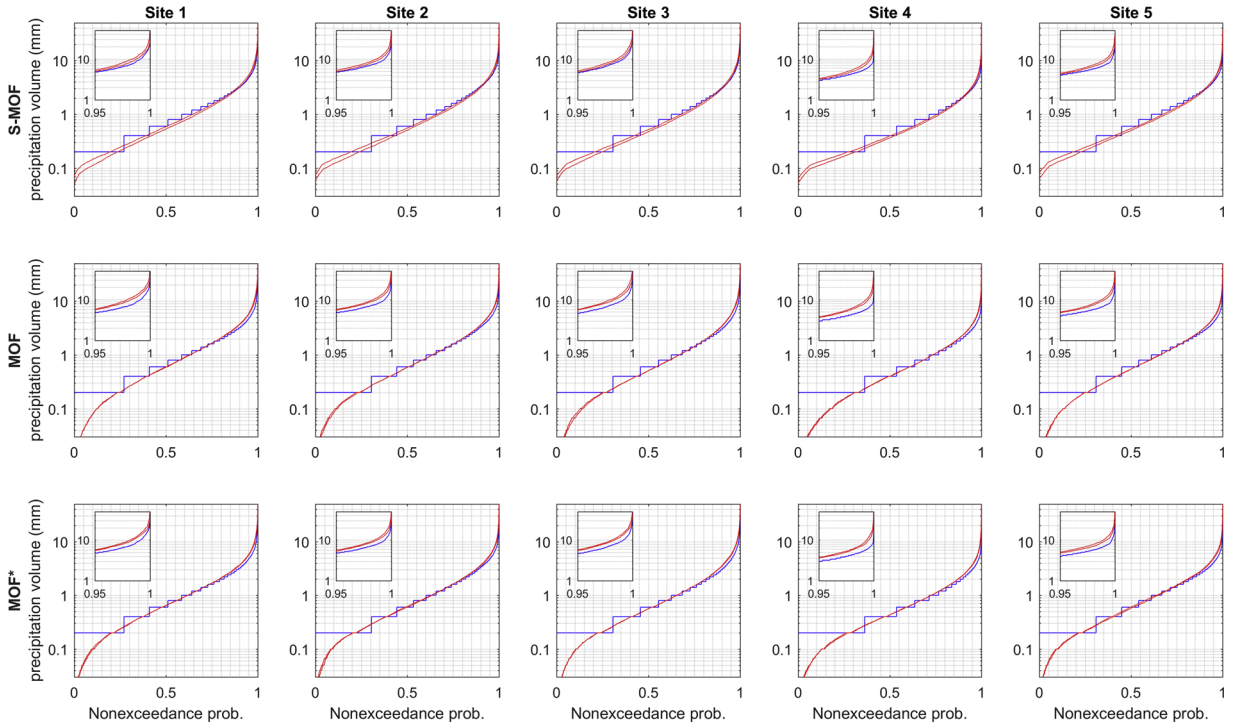

Fig. 12. Nonexceedance curves of the observed and disaggregated time series for S-MOF, MOF and MOF* (joint disaggregation of precipitation and temperature) and five selected sites across the Italian study area. Blue lines represent the observations (wet hours), red lines represent the envelope curves of the 50 simulations. The detailed plots represent the upper 5%. The sites of the plots refer to the highlighted gauges in Fig. 1. (For interpretation of the references to colour in this figure legend, the reader is referred to the web version of this article).

Declarations of interest

None.

Acknowledgements

The authors would like to thank the Swedish Research Council FORMAS for research funding, in the frame of the collaborative international consortium STEEP-STREAMS financed under the ERA-NET Cofund WaterWorks2014 Call. This ERA-NET is an integral part of the 2015 Joint Activities developed by the Water Challenges for a Changing World Joint Programme Initiative (Water JPI). This research has received funding from the European Union's Horizon 2020 research and innovation programme under the Marie Skłodowska-Curie grant agreement STARFLOOD No. 793558. The authors thank Theo Voulgaridis for help in shaping this study and Pierre Chopin for useful comments. Detailed comments by Guillaume Evin helped to improve a previous version of this manuscript. The authors also benefited from interaction with fellows within the Centre of Natural Hazards and Disaster Science (CNDS) in Sweden. The software is available as open-source Matlab code. It is provided with a tutorial and all observation data used in this article. Access is possible via the main author's github page, https://github.com/KBreinl/S-MOF. Comments by the editor and three anonymous reviewers are gratefully acknowledged.

Appendix A. Supplementary data

Supplementary material related to this article can be found, in the online version, at doi:https://doi.org/10.1016/j.ejrh.2018.12.002.

References

Apipattanavis, S., Podesta, G., Rajagopalan, B., Katz, R.W., 2007. A semiparametric multivariate and multisite weather generator. Water Resour. Res. 43 (11). https://doi.org/10.1029/2006wr005714. Artn W11401.

Arnaud, P., Bouvier, C., Cisneros, L., Dominguez, R., 2002. Influence of rainfall spatial variability on flood prediction. J. Hydrol. 260 (1-4), 216–230. https://doi.org/10.1016/S0022-1694(01)00611-4. S0022-1694(01)00611-4.

Bardossy, A., Pegram, G.G.S., 2016. Space-time conditional disaggregation of precipitation at high resolution via simulation. Water Resour. Res. 52 (2), 920–937. https://doi.org/10.1002/2015WR018037.

Bardossy, A., Plate, E.J., 1992. Space-time model for daily rainfall using atmospheric circulation patterns. Water Resour. Res. 28 (5), 1247–1259.

Blöschl, G., Sivapalan, M., 1995. Scale issues in hydrological modelling: a review. Hydrol. Processes 9 (3-4), 251–290. https://doi.org/10.1002/hyp.3360090305.
Boote, K.J., Jones, J.W., White, J.W., Asseng, S., Lizaso, J.I., 2013. Putting mechanisms into crop production models. Plant Cell Environ 36 (9), 1658–1672. https://doi.org/10.1111/pce.12119.
Borgomeo, E., Farmer, C.L., Hall, J.W., 2015. Numerical rivers: a synthetic streamflow generator for water resources vulnerability assessments. Water Resour. Res. 51 (7), 5382–5405. https://doi.org/10.1002/2014wr016827.
Brandsma, T., Buishand, T.A., 1998. Simulation of extreme precipitation in the Rhine basin by nearest-neighbour resampling. Hydrol. Earth Syst. Sci. 2 (2-3), 195–209.
Brath, A., Montanari, A., Toth, E., 2002. Neural networks and non-parametric methods for improving real-time flood forecasting through conceptual hydrological models. Hydrol. Earth Syst. Sci. 6 (4), 627–639. https://doi.org/10.5194/hess-6-627-2002.
Breinl, K., Turkington, T., Stowasser, M., 2013. Stochastic generation of multi-site daily precipitation for applications in risk management. J. Hydrol. 498, 23–35. https://doi.org/10.1016/j.jhydrol.2013.06.015.
Breinl, K., Turkington, T., Stowasser, M., 2015. Simulating daily precipitation and temperature: a weather generation framework for assessing hydrometeorological hazards. Meteorol. Appl. 22 (3), 334–347. https://doi.org/10.1002/met.1459.
Breinl, K., et al., 2017a. Can weather generation capture precipitation patterns across different climates, spatial scales and under data scarcity? Nat. Sci. Rep. 7.
Breinl, K., Strasser, U., Bates, P., Kienberger, S., 2017b. A joint modelling framework for daily extremes of river discharge and precipitation in urban areas. J. Flood Risk Manage. 10 (1), 97–114. https://doi.org/10.1111/jfr3.12150.
Buishand, T.A., Brandsma, T., 2001. Multisite simulation of daily precipitation and temperature in the Rhine basin by nearest-neighbor resampling. Water Resour. Res. 37 (11), 2761–2776. https://doi.org/10.1029/2001wr000291.
Carsteanu, A., Foufoula-Georgiou, E., 1996. Assessing dependence among weights in a multiplicative cascade model of temporal rainfall. J. Geophys. Res.-Atmos. 101 (D21), 26363–26370. https://doi.org/10.1029/96jd01657.
Clark, M.P., et al., 2004. A resampling procedure for generating conditioned daily weather sequences. Water Resour. Res. 40 (4). https://doi.org/10.1029/2003wr002747. Artn W04304.
Debele, B., Srinivasan, R., Parlange, J.Y., 2007. Accuracy evaluation of weather data generation and disaggregation methods at finer timescales. Adv. Water Resour. 30 (5), 1286–1300. https://doi.org/10.1016/j.advwatres.2006.11.009.
Di Baldassarre, G., Castellarin, A., Brath, A., 2006. Relationships between statistics of rainfall extremes and mean annual precipitation: an application for design-storm estimation in northern central Italy. Hydrol. Earth Syst. Sci. 10 (4), 589–601.
Evin, G., Favre, A.C., Hingray, B., 2018. Stochastic generation of multi-site daily precipitation focusing on extreme events. Hydrol. Earth Syst. Sci. 22 (1), 655–672. https://doi.org/10.5194/hess-22-655-2018.
Gottardi, F., Obled, C., Gailhard, J., Paquet, E., 2012. Statistical reanalysis of precipitation fields based on ground network data and weather patterns: application over French mountains. J. Hydrol. 432, 154–167. https://doi.org/10.1016/j.jhydrol.2012.02.014.
Gupta, V.K., Waymire, E.C., 1993. A statistical analysis of mesoscale rainfall as a random Cascade. J. Appl. Meteorol. 32 (2), 251–267. https://doi.org/10.1175/1520-0450(1993)032<0251:Asaomr>2.0.Co;2.
Hoch, J.M., et al., 2017. Assessing the impact of hydrodynamics on large-scale flood wave propagation - a case study for the Amazon basin. Hydrol. Earth Syst. Sci. 21 (1), 117–132. https://doi.org/10.5194/hess-21-117-2017.
Hock, R., 2003. Temperature index melt modelling in mountain areas. J. Hydrol. 282 (1-4), 104–115. https://doi.org/10.1016/S0022-1694(03)00257-9.
Johnson, M.E., Fitzpatrick, E.A., 1977. A comparison of two methods of estimating a mean diurnal temperature curve during the daylight hours. Arch. für Meteorol. Geophysik und Bioklimatologie, Serie B 25 (3), 251–263. https://doi.org/10.1007/BF02243056.
Khaliq, M.N., Cunnane, C., 1996. Modelling point rainfall occurrences with the modified Bartlett-Lewis rectangular pulses model. J. Hydrol. 180 (1-4), 109–138. https://doi.org/10.1016/0022-1694(95)02894-3.
Kottek, M., Grieser, J., Beck, C., Rudolf, B., Rubel, F., 2006. World map of the Koppen-Geiger climate classification updated. Meteorol. Z. 15 (3), 259–263. https://doi.org/10.1127/0941-2948/2006/0130.
Koutsoyiannis, D., Onof, C., 2001. Rainfall disaggregation using adjusting procedures on a Poisson cluster model. J. Hydrol. 246 (1-4), 109–122. https://doi.org/10.1016/S0022-1694(01)00363-8.
Koutsoyiannis, D., Onof, C., Wheater, H.S., 2003. Multivariate rainfall disaggregation at a fine timescale. Water Resour. Res. 39 (7). https://doi.org/10.1029/2002wr001600. Artn 1173.
Lall, U., Sharma, A., 1996. A nearest neighbor bootstrap for resampling hydrologic time series. Water Resour. Res. 32 (3), 679–693.
Leander, R., Buishand, A., Aalders, P., De Wit, M., 2005. Estimation of extreme floods of the River meuse using a stochastic weather generator and a rainfall-runoff model. Hydrol. Sci. J. 50 (6), 1089–1103. https://doi.org/10.1623/hysj.2005.50.6.1089.
Lehning, M., et al., 2006. ALPINE3D: a detailed model of mountain surface processes and its application to snow hydrology. Hydrol. Processes 20 (10), 2111–2128. https://doi.org/10.1002/hyp.6204.
Lenderink, G., Van Meijgaard, E., 2008. Increase in hourly precipitation extremes beyond expectations from temperature changes. Nat. Geosci. 1 (8), 511–514. https://doi.org/10.1038/ngeo262.
Li, X., et al., 2018. Three resampling approaches based on method of fragments for daily-to-subdaily precipitation disaggregation. Int. J. Climatol. 38, E1119–E1138. https://doi.org/10.1002/joc.5438.
Lisniak, D., Franke, J., Bernhofer, C., 2013. Circulation pattern based parameterization of a multiplicative random cascade for disaggregation of observed and projected daily rainfall time series. Hydrol. Earth Syst. Sci. 17 (7), 2487–2500. https://doi.org/10.5194/hess-17-2487-2013.
Lu, Y., Qin, X.S., 2014. Multisite rainfall downscaling and disaggregation in a tropical urban area. J. Hydrol. 509, 55–65. https://doi.org/10.1016/j.jhydrol.2013.11.027.
Luke, A., Vrugt, J.A., AghaKouchak, A., Matthew, R., Sanders, B.F., 2017. Predicting nonstationary flood frequencies: evidence supports an updated stationarity thesis in the United States. Water Resour. Res. 53 (7), 5469–5494. https://doi.org/10.1002/2016WR019676.
Markovic, D., Plavsic, J., Ilich, N., Ilic, S., 2015. Non-parametric stochastic generation of streamflow series at multiple locations. Water Resour. Manage. 29 (13), 4787–4801. https://doi.org/10.1007/s11269-015-1090-z.
Mehrotra, R., Westra, S., Sharma, A., Srikanthan, R., 2012. Continuous rainfall simulation: 2. A regionalized daily rainfall generation approach. Water Resour. Res. 48https://doi.org/10.1029/2011wr010490. Artn W01536.
Mezghani, A., Hingray, B., 2009. A combined downscaling-disaggregation weather generator for stochastic generation of multisite hourly weather variables over complex terrain: development and multi-scale validation for the Upper Rhone River basin. J. Hydrol. 377 (3-4), 245–260. https://doi.org/10.1016/j.jhydrol.2009.08.033.
Milly, P.C.D., et al., 2008. Climate change - stationarity is dead: Whither water management? Science 319 (5863), 573–574. https://doi.org/10.1126/science.1151915.
Molnar, P., Burlando, P., 2005. Preservation of rainfall properties in stochastic disaggregation by a simple random cascade model. Atmos. Res. 77 (1-4), 137–151. https://doi.org/10.1016/j.atmosres.2004.10.024.
Montanari, A., Koutsoyiannis, D., 2014. Modeling and mitigating natural hazards: stationarity is immortal!. Water Resour. Res. 50 (12), 9748–9756. https://doi.org/10.1002/2014WR016092.
Müller, H., Haberlandt, U., 2015. Temporal rainfall disaggregation with a Cascade model: from single-station disaggregation to spatial rainfall. J. Hydrol. Eng. 20 (11).
Müller, H., Haberlandt, U., 2018. Temporal rainfall disaggregation using a multiplicative cascade model for spatial application in urban hydrology. J. Hydrol.
Mutzner, R., et al., 2015. Controls on the diurnal streamflow cycles in two subbasins of an alpine headwater catchment. Water Resour. Res. 51 (5), 3403–3418. https://doi.org/10.1002/2014wr016581.
Parton, W.J., Logan, J.A., 1981. A model for diurnal-variation in soil and air-temperature. Agric. Meteorol. 23 (3), 205–216. https://doi.org/10.1016/0002-1571(81)90105-9.
Porter, J.R., Semenov, M.A., 2005. Crop responses to climatic variation. Philos. Trans. R. Soc. B 360 (1463), 2021–2035. https://doi.org/10.1098/rstb.2005.1752.

Pui, A., Sharma, A., Mehrotra, R., Sivakumar, B., Jeremiah, E., 2012. A comparison of alternatives for daily to sub-daily rainfall disaggregation. J. Hydrol. 470, 138–157. https://doi.org/10.1016/j.jhydrol.2012.08.041.

Reynolds, J.E., Halldin, S., Xu, C.Y., Seibert, J., Kauffeldt, A., 2017. Sub-daily runoff predictions using parameters calibrated on the basis of data with a daily temporal resolution. J. Hydrol. 550, 399–411. https://doi.org/10.1016/j.jhydrol.2017.05.012.

Rigon, R., Bertoldi, G., Over, T.M., 2006. GEOtop: a distributed hydrological model with coupled water and energy budgets. J. Hydrometeorol. 7 (3), 371–388. https://doi.org/10.1175/Jhm497.1.

Rodriguez-Iturbe, I., Cox, D.R., Isham, V., 1987. Some models for rainfall based on stochastic Point-processes. Proc. R. Soc. Lond. Ser.-A 410 (1839), 269–288. https://doi.org/10.1098/rspa.1987.0039.

Serinaldi, F., Kilsby, C.G., 2015. Stationarity is undead: uncertainty dominates the distribution of extremes. Adv. Water Resour. 77, 17–36. https://doi.org/10.1016/j.advwatres.2014.12.013.

Sharma, A., Srikanthan, S., 2006. Continuous rainfall simulation: a nonparametric alternative. 30th Hydrology & Water Resources Symposium: Past, Present & Future. Conference Design. pp. 86.

Sikorska, A.E., Seibert, J., 2018. Appropriate temporal resolution of precipitation data for discharge modelling in pre-alpine catchments. Hydrol. Sci. J. 63 (1), 1–16. https://doi.org/10.1080/02626667.2017.1410279.

Simoni, S., et al., 2011. Hydrologic response of an alpine watershed: application of a meteorological wireless sensor network to understand streamflow generation. Water Resour. Res. 47https://doi.org/10.1029/2011wr010730. Artn W10524.

Skoien, J.O., Blöschl, G., Western, A.W., 2003. Characteristic space scales and timescales in hydrology. Water Resour. Res. 39 (10). https://doi.org/10.1029/2002wr001736. Artn 1304.

Stephenson, D.B., et al., 1999. Extreme daily rainfall events and their impact on ensemble forecasts of the Indian monsoon. Mon. Weather Rev. 127 (9), 1954–1966. https://doi.org/10.1175/1520-0493(1999)127<1954:Edreat>2.0.Co;2.

Tetzlaff, D., Uhlenbrook, S., 2005. Significance of spatial variability in precipitation for process-oriented modelling: results from two nested catchments using radar and ground station data. Hydrol. Earth Syst. Sci. 9 (1-2), 29–41. https://doi.org/10.5194/hess-9-29-2005.

Villarini, G., Serinaldi, F., Krajewski, W.F., 2008. Modeling radar-rainfall estimation uncertainties using parametric and non-parametric approaches. Adv. Water Resour. 31 (12), 1674–1686. https://doi.org/10.1016/j.advwatres.2008.08.002.

Wang, Y., He, B., Takase, K., 2009. Effects of temporal resolution on hydrological model parameters and its impact on prediction of river discharge. Hydrol. Sci. J. 54 (5), 886–898. https://doi.org/10.1623/hysj.54.5.886.

Warscher, M., et al., 2013. Performance of complex snow cover descriptions in a distributed hydrological model system: a case study for the high alpine terrain of the Berchtesgaden Alps. Water Resour. Res. 49 (5), 2619–2637. https://doi.org/10.1002/wrcr.20219.

Wasko, C., Sharma, A., 2015. Steeper temporal distribution of rain intensity at higher temperatures within Australian storms. Nat. Geosci. 8 (7). https://doi.org/10.1038/Ngeo2456. 527-U166.

Westra, S., Mehrotra, R., Sharma, A., Srikanthan, R., 2012. Continuous rainfall simulation: 1. A regionalized subdaily disaggregation approach. Water Resour. Res. 48https://doi.org/10.1029/2011wr010489. Artn W01535.

Wilks, D.S., 1998. Multisite generalization of a daily stochastic precipitation generation model. J. Hydrol. 210 (1-4), 178–191. https://doi.org/10.1016/S0022-1694(98)00186-3.

Wilks, D.S., 1999. Multisite downscaling of daily precipitation with a stochastic weather generator. Clim. Res. 11 (2), 125–136. https://doi.org/10.3354/Cr011125.

Wojcik, R., Buishand, T.A., 2003. Simulation of 6-hourly rainfall and temperature by two resampling schemes. J. Hydrol. 273 (1-4), 69–80. https://doi.org/10.1016/S0022-1694(02)00355-4. Pii S0022-1694(02)00355-4.

Zhang, J., Han, D.W., 2017. Assessment of rainfall spatial variability and its influence on runoff modelling: a case study in the Brue catchment, UK. Hydrol. Processes 31 (16), 2972–2981. https://doi.org/10.1002/hyp.11250.